Ore Geology Reviews 95 (2018) 161–181

Contents lists available at ScienceDirect

Ore Geology Reviews

journal homepage: www.elsevier.com/locate/oregeorev

Petrogenesis of *syn*-orogenic rare metal pegmatites in the Chinese Altai: Evidences from geology, mineralogy, zircon U-Pb age and Hf isotope

Zheng-Hang Lv[a], Hui Zhang[a,*], Yong Tang[a], Yun-Long Liu[a], Xin Zhang[b]

[a] Key laboratory of High-temperature and High-pressure Study of the Earth's Interior, Institute of Geochemistry, Chinese Academy Sciences, Guiyang 550081, China
[b] School of Earth Sciences and Gansu Key Laboratory of Mineral Resources in Western China, Lanzhou University, Lanzhou 730000, China

ARTICLE INFO

Keywords:
Petrogenesis
Syn-orogenic
Rare metal
Pegmatite
Chinese Altai

ABSTRACT

Recently, an increasing number of anatetic pegmatites have been confirmed. In contrast to the granitic pegmatite, the anatetic pegmatite has no relation to granite. It is therefore necessary to reacquaint the origin and classification of pegmatitic rocks. As one of the largest pegmatite provinces, the Chinese Altai provides a natural laboratory for pegmatite study. To date, the type, age, source and tectonic setting of the *syn*-orogenic pegmatites in the Chinese Altai remain unclear. In this work, the CMS (Chemical composition-Mineral assemblage-Structural geology) classification is primarily applied on the pegmatitic rocks in the Chinese Altai. Five types' pegmatitic rocks, including metapegmatite, pegmatoid, pegmatite, pseudopegmatite and granite pegmatite, are identified by their CMS features. In addition, the geology, mineralogy, zircon U-Pb ages and Hf isotopes of six pegmatites are presented in this work. The pegmatites, numbered JMHB02, QBL02, TLT01, ALJK01, AMLG01 and TMLT01, are dated at 394.8 ± 4.0 Ma, 402.6 ± 5.5 Ma, 385.9 ± 3.5 Ma, 368.0 ± 4.0 Ma, 358.3 ± 4.6 Ma and 333.0 ± 6.0 Ma, respectively, indicating that they were formed during the *syn*-orogenic stage of the Altai orogenic process. They are exposed in the Qiongkuer domain in the southern Chinese Altai, juxtaposed with the late- and/or post-orogenic pegmatites in the same pegmatite field. No parental granite can be confirmed for all these pegmatites. Comparatively, the synorogenic pegmatites are scarce, and have lower mineralization grades than the late- and postorogenic pegmatites. Zircon Hf isotopic compositions of the *syn*-orogenic pegmatites have positive $\varepsilon_{Hf}(t)$ values of +2.06–+8.28 and old T_{DM2} ages of 1,234–860 Ma and are consistent with those of most of the *syn*-orogenic I- and S-granites, which indicates that the pegmatites and granites have a common immature crustal source from the early Paleozoic metasedimentary rocks. Compared to the post-orogenic pegmatites in the Central Altai domain, the *syn*-orogenic pegmatites in this work have larger positive $\varepsilon_{Hf}(t)$ values and younger T_{DM2} ages, indicating that more juvenile components were involved in their magma sources. Combining this study with previous works, we suggest that the anatexis of metasediments induced by decompression and injection of heat energy and mantle-derived materials under a forearc extensional setting led to the formation of the *syn*-orogenic pegmatites in the Chinese Altai.

1. Introduction

Pegmatite is known for its advantages in quantity and mineralization potential for rare-metal ore deposits and is commonly characterized by large sizes of mineral specimens, peculiar textures (e.g., skeleton and graphic) and internal zonation. Although pegmatite has been studied for approximately two centuries, two critical points about the petrogenesis of pegmatite, including the generation of pegmatite-forming melt and internal zonation, remain unclear and under debate. For the first point, the typical view suggests that the pegmatite-forming melt originates from the differentiation of granitic melt (Černý, 1991a; Černý and Ercit, 2005; Černý et al., 2012a). However, for most studied pegmatites in worldwide, including the Tanco pegmatite from Canada, the Greenbush pegmatite from Australia and the Koktokay No. 3 pegmatite from China, the parental granites have not yet been found and confirmed. For the second point, the J-B model (Jahns and Burnham, 1969) suggests that saturation of the aqueous vapor phase and alkali fractionation between the melt and vapor are responsible for mineral textural zoning in pegmatite. In contrast, London and co-workers propose that the contents and roles of volatiles in pegmatite formation are limited but that melt undercooling and constitutional zone refining (CZR) are the core steps to the internal zonation in pegmatite (London, 2005; 2008; 2014).

Today, the classification of pegmatite into LCT, NYF and mixed

* Corresponding author.
E-mail address: Zhanghui@mail.gyig.ac.cn (H. Zhang).

https://doi.org/10.1016/j.oregeorev.2018.02.022
Received 11 September 2017; Received in revised form 9 February 2018; Accepted 13 February 2018
Available online 14 February 2018
0169-1368/

petrogenetical families (Černý, 1991a; Černý and Ercit, 2005) is accepted worldwide. The LCT pegmatite is commonly suggested to be associated with I- or S-type granite derived from a sedimentary source in a late- or post-orogenic setting, and the NYF pegmatite is proposed to be associated with A-type granite derived from a mixed source of lower crust and mantle in a post- or anorogenic setting (Černý, 1991b; Černý et al., 2012a). However, a mass of pegmatites have been proved to be anatexis origin in recent years (Martin and De Vito, 2005; Martin, 2007; Dill, 2015a, b, 2016, 2018; Müller et al., 2016; Simmons, 2016; Simmons and Falster, 2016), and they have no petrogenetic relation to the neighboring granite(s). Therefore, previous classifications are no longer suitable for these granite-unrelated pegmatites, and it is necessary to reacquaint the origin and classification of pegmatitic rocks. The age statistics on pegmatites worldwide suggest that LCT pegmatite is commonly formed during the post-orogenic stage (McCauly and Bradley, 2014; Bradley and McCauly, 2016), which demonstrates the significance of late- to post-tectonic setting for the generation of LCT pegmatite. However, the petrogenesis of *syn*-orogenic pegmatite is rarely studied due to its smaller numbers and lower mineralization potential compared with post-orogenic pegmatite (Černý, 1991b; Tkachev, 2011; Bradley and McCauly, 2016).

The Altai Orogenic Belt is one of the largest Phanerozoic pegmatite provinces in the world. As an important part of it, the Chinese Altai is known for abundant pegmatitic rocks and associated rare-metal deposits. According to previous statistics, there are approximately one hundred thousand pegmatite dykes developed in an area of ~20,000 km^2 (Zou and Li, 2006), which makes the Chinese Altai an ideal natural laboratory for pegmatite study. However, the previous classifications (Zou and Xu, 1975; Xu and Zou, 1975; Wu and Zou, 1989) are hard to cover all types of these pegmatitic rocks, and lots of granite-unrelated pegmatites have been ascribed to the differentiation product of granites, which impede the understanding of their origins. Besides, some pegmatites' ages given by Ar-Ar or Rb-Sr may lead to limited understanding of pegmatite. For example, the Koktokay No. 3 pegmatite, the largest and richest pegmatite in the Chinese Altai, was suggested to have formed in the Jurassic according to muscovite and microcline Ar-Ar ages (178–148 Ma, Chen et al., 1999; 195–173 Ma, Zhou et al., 2015), which leads to the conclusion that the rare-metal metallogeny reached its peak in the Jurassic in an anorogenic setting (Wang et al., 2004; Zhou et al., 2015, 2016). Based on zircon and columbite-group U-Pb methods, recent geochronological work has revealed that the pegmatites mainly formed in the late Paleozoic-early Mesozoic (280–180 Ma) (Zhu et al., 2006; Wang et al., 2007; Ren et al., 2011; Lv et al., 2012, 2015; Qin et al., 2013; Liu et al., 2014; Ma et al., 2015; Liu, 2015; Zhang et al., 2016; Zhou et al., 2016; Liu et al., 2017), with the formation and mineralization peaks in the Triassic post-orogenic setting, represented by the formation of the super-large Li-Be-Ta-Nb-Cs ore deposit hosted in the Koktokay No. 3 pegmatite (220–210 Ma, Zhu et al., 2006; Wang et al., 2007; Chen, 2011; Liu et al., 2014; Che et al., 2015), the super-large Li ore deposit hosted in the Kaluan No. 650, 805, 806 and 807 pegmatites (227–211 Ma, Ma et al., 2015), and the large Li-Be-Ta-Nb ore deposit hosted in the Kelumute No. 112 pegmatite (238–210 Ma, Lv et al., 2012). In this work, the geology, mineralogy, zircon U-Pb ages and Hf isotopes of six *syn*-orogenic rare metal pegmatites are presented. Combine with previous works, in order to clarify the petrogenesis of the scarce *syn*-orogenic pegmatites in the Chinese Altai, and also try to apply the CMS (Chemical composition-Mineral assemblage-Structural geology) classification (Dill, 2015a, b; 2016) on the pegmatitic rocks in this region.

2. Geological background

2.1. Regional geology

The Chinese Altai occupies a key position within the Central Asian Orogenic Belt (CAOB) (Fig. 1a), and its geodynamic evolution is closely associated with that of the CAOB (Hu et al., 2000; Xiao et al., 2004; Han et al., 2014). The Chinese Altai is divided into four fault-bounded domains based on stratigraphy, metamorphism, deformation pattern and magmatic activity, including the North Altai domain, the Central Altai domain, the Qiongkuer domain and the Erqis domain (Fig. 1b) (Yuan et al., 2007; Long et al., 2007; Sun et al., 2008; Cai et al., 2011a,b). The North Altai domain (Unit I in Fig. 1b) is bounded to the south by the Hongshanzui-Nuoerte Fault and consists of Devonian to Lower Carboniferous metavolcanic and metasedimentary rocks (Windley et al., 2002; Wang et al., 2006) and Devonian granite porphyry and I-type granites (Yuan et al., 2001; Lv et al., 2015; Qin et al., 2016). The Central Altai domain (Unit II in Fig. 1b) is bounded by the Hongshanzui-Nuoerte Fault to the north and the Abagong-Kuerti Fault to the south. It is composed of a thick turbiditic and pyroclastic sequence (Habahe Group) (BGMRX, 1993; Windley et al., 2002), upper Ordovician volcanic molasse and terrigenous clastic sequences (Dongxileke and Baihaba Formations), and middle to upper Silurian metasandstone (Kulumuti Formation) (BGMRX, 1993; Windley et al., 2002). I- and S-type granitoids are widely exposed in this domain and have ages ranging from early Paleozoic to early Mesozoic with a peak age in the Devonian (Zhao et al., 1993; Chen and Jahn, 2002; Tong et al., 2006a,b, 2007; 2012, 2014; Wang et al., 2006, 2009, 2010, 2014a; Windley et al., 2007; Yuan et al., 2007; Sun et al., 2008, 2009; Cai et al., 2011a, b, 2012, 2016; Liu, 2015; Ma et al., 2015; Zhang et al., 2017a). Mafic rocks that formed in the Devonian have limited distribution in the Ashele and Koktokay areas (Cai et al., 2010, 2012b). Some researchers suggest that the Central Altai may include a part of the Altai-Mongolian microcontinent (Windley et al., 2002; Li et al., 2006; Wang et al., 2009; Zhang et al., 2017a). The Qiongkuer domain (Unit III in Fig. 1b) is bounded by the Abagong-Kuerti Fault to the north and the Fuyun-Xibodu Fault to the south, and is composed of late Paleozoic clastic and volcanic rocks, which are subdivided into the early Devonian Kangbutiebao Formation and mid-Devonian Altai Formation, respectively (BGMRX, 1993; Windley et al., 2002). Igneous rocks in this domain mainly include middle-late Paleozoic I-type granite (Wang et al., 2006, 2009, 2010; Yuan et al., 2007; Sun et al., 2008; Yang et al., 2010; Zheng et al., 2016), late Paleozoic A-type granite (Tong et al., 2014; Liu et al., 2017), and Devonian-Permian mafic dykes (Pirajno et al., 2008; Cai et al., 2010, 2016). The Erqis domain (Unit IV in Fig. 1b) is located between the Fuyun-Xibodu Fault to the north and the Erqis Fault to the south. It is mainly composed of Devonian fossiliferous successions (Kangbutiebao Formation) that are, in turn, overlain by late Carboniferous formations (BGMRX, 1993; Windley et al., 2002). A few Carboniferous-Permian granites are also exposed in this domain (Tong et al., 2012, 2014).

The Chinese Altai has been variously ascribed to a passive continental margin (He et al., 1990), a subductuion-accretion complex (Sengor et al., 1993) or a Precambrian micro-continent (e.g., Li et al., 2006). However, recent studies support that the Chinese Altai is a Middle Cambrian to Early Permian magmatic arc formed by a continuous subduction-accertion process at an active margin (e.g., Windley et al., 2002; Xiao et al., 2003, 2008, 2015; Long et al., 2007, 2010; Yuan et al., 2007; Sun et al., 2008; Cai et al., 2011a,b; 2012a,b; 2016). The oldest arc volcanic rhyodacite (505 ± 2 Ma, Windley et al., 2002) and granite (507.2 ± 5.5 Ma, Zhang et al., 2017b) confirmed so far indicate that a continental magmatic arc was formed in the Chinese Altai during the middle Cambrian. The subsequent subduction-accertion process is also recorded by the Ordovician and Silurian volcanic rocks, mafic complexes and granitic rocks (Wang et al., 2006; Sun et al., 2008; Cai et al., 2011a; Wong et al., 2010; Wang et al., 2011; Zhang et al., 2017b). During the Devonian period, the adakite, boninite, low-TiO_2 and high-TiO_2 basalt and high-Mg andesite are ascribed to magmatic arc productions (Niu et al., 1999; 2006). The contemporary volcanic dacite-rhyolite suite, gabbros, dolerites granites and low-pressure/high-temperature metamorphism indicate an oceanic ridge subduction regime in the Chinese Altai (Sun et al., 2008; Cai et al., 2010, 2012b;

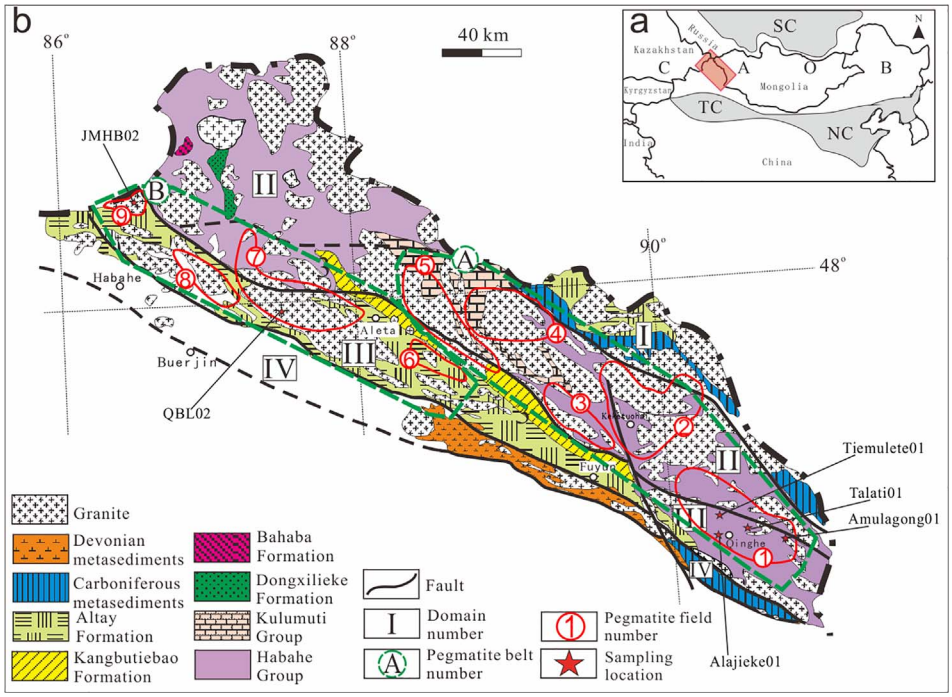

Fig. 1. Tectonic location (a) and geological sketch map of the Chinese Altai (b) (modified from Windley et al., 2002). Abbreviation: CAOB = Central Asian Orogenic Belt; SC = Siberia Craton; TC = Tarim Craton; NC = North China Craton. Code: I, North Altai domain; II, Central Altai Domain; III, Qiongkuer domain; IV, Erqis domain. A, Halong-Qinghe pegmatite belt; B, Jiamanhaba-Xiaokalasu pegmatite belt. ①, Qinghe pegmatite field; ②, Koktokay pegmatite field; ③, Kuwei-Jiebiete pegmatite field; ④, Kelumute-Jideke pegmatite field; ⑤, Kalaeerqisi pegmatite field; ⑥, Dakalasu-Kekexier pegmatite field; ⑦, Xiaokalasu-Qiebielin pegmatite field; ⑧, Hailiutan-Yeliuman pegmatite field; ⑨, Jiamanhaba pegmatite field.

Jiang et al., 2010; Wang et al., 2011). Meanwhile, an extensional forearc basin was formed in the southern of Chinese Altai, according to the systematic studies of zircon U-Pb age, whole rock compositions and Sr-Nd istope on granites (Sun et al., 2008; Yuan et al., 2007) and formations of a series of fault-depression basins, such as Ashele, Chonghuer, Kelan and Maizi basins (Yang et al., 2013). The extensional setting lasted to the late Carboniferous at least (Yuan et al., 2007). After that, the East Junggar arc was docked to the Mongolia collage system in the early Permian, and the active margin was changed into a back-arc setting. A sequence of tectonic-magmatic-metamorphic events have been recorded by the Klatongke mafic intrusions and corresponding Cu-Ni ore deposits (Li et al., 2012a), intermediate-mafic dikes (Cai et al., 2016), abundant A-type granites (Han et al. 1997; Briggs et al., 2007; Tong et al. 2012; Liu et al., 2017), and high-temperature metamorphism (Chen et al., 2006; Hu, 2006; Briggs et al., 2007, 2009; Li et al., 2014). Finally, the Tarim craton collided with the Siberia craton in Triassic (Xiao et al., 2009, 2015; Lv et al., 2012; Zheng et al., 2015).

2.2. Geology of pegmatite fields and the studied pegmatites

There are approximately 100,000 pegmatite dykes distributed in two pegmatite belts and nine pegmatite fields in the Chinese Altai. The Halong-Qinghe pegmatite belt ('A' in Fig. 1b) is located in the Central Altai domain and consists of five pegmatite fields: Qinghe, Kuwei-Jiebiete, Keketuohai, Kelumute-Jideke and Kalaeerqisi (Numbered ① to ⑤ in Fig. 1b). In addition, the Jiamanhaba-Dakalasu pegmatite belt ('B' in Fig. 1b) is located in the Qiongkuer domain and consists of four pegmatite fields: Dakalasu-Kekexier, Xiaokalasu-Qiebielin, Hailiutan-Yeliuman and Jiamanhaba (Numbered ⑥ to ⑨ in Fig. 1b) (Wu and Zou, 1989).

2.2.1. Jiamanhaba pegmatite field

It is located in the northwestern part of the Chinese Altai, close to the national boundary between China and Kazakhstan and adjacent to Ashele Basin to the south (Fig. 1b). Tectonically, it is situated in the western end of the Kabaer-Xibodu Paleozoic magmatic arc and the north limb of Baogutu anticlinorium. The area is dominated by igneous rocks including Caledonian biotite granite and plagiogranite, which are intruded by lots of pegmatites. In addition, late Variscan two-mica granite is also exposed in the southern of the field (Zou and Li, 2006). As the secondary host rock, the lower to mid-Devonian Tuokesalei Formation mainly consists of marine terrigenous clastics with siliceous and carbonate rocks and shows limited outcrop in the central area (Yang et al., 2013). Pegmatites in this field have scattered distribution and limited scales with lengths and widths no more than 500 m and 10 m, respectively. They are also characterized by low fractionation grade, simple internal zoning and mineralization of Be ± muscovite. The investigated JMHB02 pegmatite intruded into the biotite granite along a northwest joint (Fig. 2a), with an outcrop of 110 m in length and 2.5 m in width, a strike of WNW 280° and a dip angle of 50°. From the exocontact to the core zone, there is symmetrical development of a chilled border (~5% vol.), graphic texture zone (~20% vol.), blocky microcline zone (~40% vol.) and blocky quartz zone (~35% vol.). Tourmalinization is observed in the exocontact of the wall rock. Beryl mineral is mainly hosted in the graphic texture zone (Fig. 2b). Besides that, other accessory minerals are rare (Table 1). According to the CMS classification in the long version (Dill, 2015a, b), it is denominated as a biotite granite-hosted tabular-zoned Nb-P-B-Be-muscovite-quartz-Ca-Na-K feldspar pegmatite.

2.2.2. Xiaokalasu-Qiebielin pegmatite field

It is located in the northwestern section of the Aletai district and adjacent to the Hailiutan-Yeliuman pegmatite field to the west (Fig. 1b). Tectonically, it is situated in the western of the Kabaer-Xibodu Paleozoic magmatic arc and the axis structure zone of Qiebielin anticlinorium (Zou and Li, 2006). Igneous and metasedimentary rocks have wide exposure in this pegmatite field. The former mainly consist of a large biotite granite batholith characterized by gneissic structure and intruded by small two-mica granite and muscovite granite plutons (Wang et al., 2006). The biotite granite and two-mica granite are dated at 432 ± 7 Ma (Cai et al., 2011b) and 278.6 ± 3.5 Ma (Li et al., 2012b) by zircon U-Pb, respectively. The biotite granite is the major host rock of pegmatites in the field. The metasedimentary rocks are identified as the upper to mid-Ordovician Kalaqiaola Formation, which consists of metasandstone, leptynite, schist and gneiss. Thousands of pegmatites, appearing as tabular, lens or vein, are distributed in the biotite granite and the metasedimentary rocks. Most of them have a consistent strike of NNW 330°–350° and varying scales with lengths

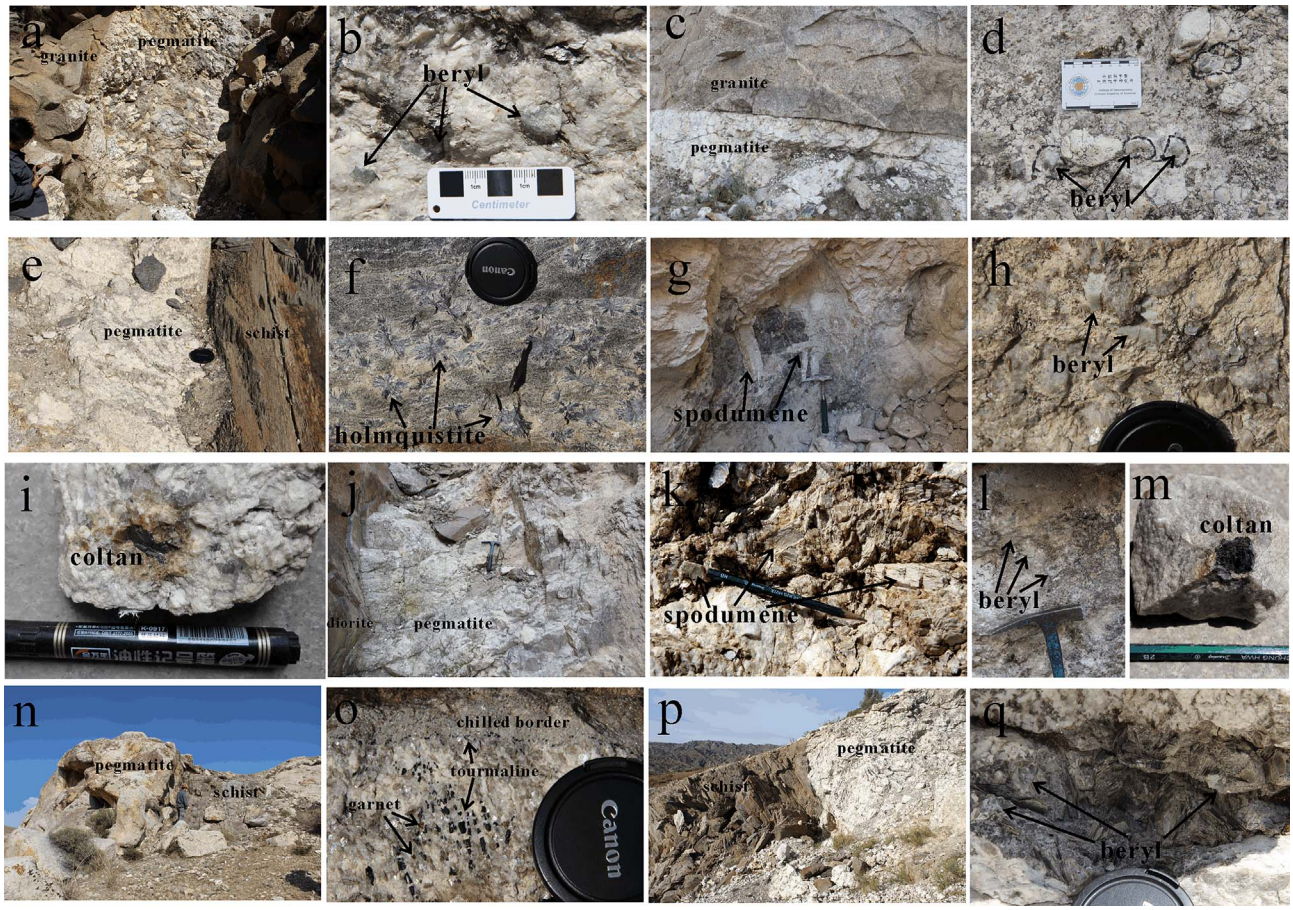

Fig. 2. The field photographs of studied pegmatites. (a), (c), (e), (j), (n) and (p) show the outcrops of the Jiamahaba pegmatite (JMHB02), the Qiebielin pegmatite (QBL02), the Talati pegmatite (TLT01), the Amulagong pegmatite (AMLG01), the Alajieke pegmatite (ALJK01) and the Tiemulete pegmatite (TMLT01), and sharp contact relationships between the pegmatites and their wall rocks; (b), (d), (h), (l) and (q) show the occurrence of beryl minerals; (g) and (k) show the occurrence of spodumene minerals; (i) and (m) show the occurrence of coltan minerals; (f) shows the holmoustitization in contact zone between the Talati pegmatite and wall rock; (o) shows the chilled border between the Alajieke pegmatite and wall rock, and tourmaline and spessartite minerals in the outer zone.

ranging from tens to hundreds of meters and widths ranging from tens of centimeters to several meters. The pegmatites commonly consist of a graphic zone, blocky microcline zone and quartz-muscovite zone. Most pegmatites contain a certain amount of beryl, muscovite and tourmaline ore minerals; only several pegmatites host small Li-Be-Nb-Ta or *gem*-grade elbaite ore deposits with distributions in Xiaokalasu or Moshega mining areas. The QBL02 pegmatite is located in the Qiebielin mining area and intruded into the gneissic biotite granite (Fig. 2c). It hosts a small beryl ore deposit and shows a strike of NNW 340°, length of 200 m and width of 20 m. The textural zones in this pegmatite include a graphic zone (~22% vol.), quartz-muscovite-microcline zone (~20% vol.), blocky microcline zone (~27% vol.), nested quartz-muscovite zone (~15% vol.), saccharoidal albite zone (~10% vol.) and quartz-muscovite-cleavelandite zone (~6% vol.). Coarse-grained beryl mineral is observed mainly in the graphic and blocky microcline zones (Fig. 2d). Other ore minerals such as tantalite-(Mn) and columbite-(Fe) and -(Mn) (Table 1) are also observed but rare. According to the CMS classification (Dill, 2015a,b), it is denominated as a gneissic biotite granite-hosted tabular-zoned (Nb-P)-B-Be-muscovite- quartz-Ca-Na-K feldspar pegmatite.

2.2.3. Qinghe pegmatite field

It is located in the southeastern part of the Chinese Altai geographically (Fig. 1b) and the plunging crown of Qinggeli anticlinorium tectonically (Zou and Li, 2006). The field consists of tens of mining areas and eight thousand pegmatite dykes. The corresponding Be ore deposits are mainly distributed in the Asikaerte, Amulagong, Talati and Buleke mining areas; Li ± Nb-Ta ± Cs ore deposits are mainly concentrated in the Baicheng, Amulagong and Talati mining areas; and muscovite ore deposits are concentrated in the Tiemulete, Buleke, Naransala and Akebulake mining areas.

2.2.4. Talati pegmatite mining area

It is located in the midportion of axis structure zone of Qinggeli anticlinorium tectonically. Metasedimentary rocks are widely exposed in this area and consist of the upper and middle Ordovician Habahe Formation. The former is composed of andalusite-biotite-quartz schist and biotite-quartz schist and has wide exposure in the southern, eastern and western parts of the area. The latter consists mainly of greenschist and has local exposure in the northern part of the area. There are approximately 60 pegmatites distributed in the biotite-quartz schist characterized by epidotization, siliconization, tourmalinization, muscovitization and holmoustitization. These pegmatites commonly show vein-like or tabular and limited outcrops with lengths no more than 200 m and widths less than 5 m. The TLT01 pegmatite is intruded into the biotite-quartz schist (Fig. 2e) with local holmoustitization observed in the exocontact zone (Fig. 2f) and hosts a small Li-Be-Ta-Nb-Cs ore deposit (Fig. 2 g, h and i). The outcrop has a length of 105 m and width of 4–8 m with a strike of WNW 310° and dip angle of 40°. It consists of complex textural zones including a blocky microcline zone (~30% vol.), quartz-muscovite zone (~15% vol.), saccharoidal albite zone (~20% vol.), cleavelandite zone (~10% vol.) and quartz-spodumene zone (~25% vol.). According to its structure-mineral-chemistry figures (Table 1), this pegmatite is denominated as a biotite-quartz-schist-

Table 1
The CMS classification of the studied pegmatitic rocks from the Chinese Altai.

Number	Pegmatite type	Host rock	Shape	Structure	Internal structure	Chemical qualifier	Mineralogical qualifier
JMHB02	Pegmatite	Biotite granite	Tabular	Baogutu anticlinorium	Zoned	Nb-P-B-Be	Microcline, quartz, muscovite, albite, anorthose, beryl, spessartine, tourmakine-(Fe), fluorapatite, zircon, gahnite, columbite-(Fe) and -(Mn), tantalite-(Mn)
QBL02	Pegmatite	Gneissic biotite granite	Tabular	Qiebielin anticlinorium	Zoned	Nb-P-B-Be	Microcline, quartz, muscovite, albite, anorthose, beryl, spessartine, tourmakine-(Fe), fluorapatite, zircon, hafnian-zircon, gahnite, columbite-(Fe) and -(Mn), tantalite-(Mn)
TLT01	Pegmatite	Biotite-quartz schist	Tabular	Qinggeli anticlinorium	Zoned	P-Cs-Nb-Be-Li	Albite, quartz, microcline, muscovite, anorthose, spodumene, beryl, tantalite-(Mn), columbite-(Mn) and -(Fe), fluorapatite, spessartine, tourmakine-(Fe), trilithionite, lithiophilite, amblygonite, hluorcalciomicrolite, hydroxymanganopyrochlore, zircon, hafnian-zircon, gahnite
AMLG01	Pegmatite	Diorite	Tabular	Qinggeli anticlinorium	Zoned	P-Cs-Nb-Be-Li	Albite, quartz, microcline, muscovite, anorthose, spodumene, beryl, tantalite-(Mn), columbite-(Mn) and -(Fe), fluorapatite, spessartine, tourmakine-(Fe), trilithionite, lithiophilite, amblygonite, zircon, hafnian-zircon, hluorcalciomicrolite, hydroxymanganopyrochlore, gahnite
ALJK01	Pegmatite	Biotite-quartz schist	Lens	Qinggeli anticlinorium	Unzoned	(F)-P-B	Microcline, quartz, muscovite, albite, anorthose, tourmakine-(Fe), spessartine, fluorapatite, zircon
TMLT01	Pegmatite	Biotite-plagioclase gneiss	Stock	Buleke overturned anticline	Zoned	(F)-Nb-P-B-Be	Microcline, muscovite, quartz, albite, anorthose, beryl, spessartine, tourmakine-(Fe), fluorapatite, zircon, gahnite, columbite-(Fe) and -(Mn), tantalite-(Mn)

hosted tabular-zoned P-Cs-Nb-Be-Li-muscovite-quartz-Ca-K-Na feldspar pegmatite.

2.2.5. Amulagong pegmatite area

It is located in the eastern section of axis structure zone of Qinggeli anticlinorium tectonically and is bounded by the Mierikete Fault and the Bageleqi-Keketuomusike Fault. Igneous rocks consist of an early Variscan diorite and a middle Variscan porphyritic biotite granite. The latter is widely exposed in the area, and the former shows local exposures within the latter. As the dominant host rock, the diorite hosts 116 pegmatite veins in its joints. General siliconization, tourmalinization and muscovitization are observed in the exocontacts of the host rock. These pegmatites show lens-, tabular-, vein- or branch-like shapes and limited outcrops with lengths less than 300 m and widths less than 5 m. The AMLG01 pegmatite is intruded into a joint of the diorite (Fig. 2j) and has a length of 150 m and width of 2–5 m, a strike of WNW 290° and dip angles of 62° for the hanging wall and 75° for the footwall. It hosts a small Li-Be-Ta-Nb ore deposit (Fig. 2 k, l and m) and consists of six textural zones, including a graphic zone (~12% vol.), blocky microcline zone (~20% vol.), quartz-muscovite zone (~18% vol.), saccharoidal albite zone (~13% vol.), quartz-spodumene zone (~20% vol.), cleavelandite zone (~12% vol.) and quartz core (~5% vol.). Similar structure-mineral-chemistry figures to the TLT01 pegmatite (Table 1), this pegmatite is also denominated as a biotite-quartz-schist-hosted tabular-zoned P-Cs-Nb-Be-Li- muscovite-quartz-Ca-K-Na feldspar pegmatite.

2.2.6. Alajieke pegmatite area

It is located in the southwestern part of the Qinghe pegmatite field geographically and the subsidiary anticline of Qinggeli anticlinorium tectonically. Hundreds of pegmatites are distributed in this area and intruded into the upper Ordovician Habahe Formation biotite-quartz schist with abrupt contacts between pegmatites and wall rocks. These pegmatites are shaped as lenses, veins or branches and have lengths of 100–200 m and widths of 2–10 m. They commonly show varying strikes, simple internal zoning and limited rare-metal mineralization. The ALJK01 pegmatite is intruded into the biotite-quartz schist (Fig. 2n), and shows a lens shape with length of 150 m, maximum width of 20 m, strike of WNW 300° and dip angle of 72°. The pegmatite has no evident internal zonation and is mainly composed of medium- to fine-grained (0.5–3 cm) microcline, quartz and muscovite with local developments of graphic and blocky (ca. 10 cm) microcline and quartz intergrowth in rim and core zones, respectively. Fine-grained (less than1 cm) tourmaline-(Fe) and almandine-spessartite minerals (Fig. 2o) are abundant in this pegmatite. According to its structure-mineral-chemistry figures (Table 1), this pegmatite is denominated as a biotite-quartz-schist-hosted lens-unzoned F-P-B-muscovite-quartz-Ca-K-Na feldspar pegmatite.

2.2.7. Tiemulete pegmatite area

It is located in the central area of the Qinghe pegmatite field. Tectonically, it is situated in the core of the Buleke overturned anticline, which is regarded as the main ore-controlling structure. Igneous rock mainly consists of an early Variscan diorite, has local exposure in the northern and eastern parts of the area, and hosts tens of beryl-bearing pegmatites. As the dominant host rock, the lower to mid-Ordovician Habahe Formation consists of garnet-biotite gneiss, sillimanite-two mica gneiss, augen gneiss, striped, enterolithic and augen migmatite and biotite-plagioclase gneiss. It is intruded by approximately two hundred pegmatites, including 40 muscovite mineralization pegmatites and 28 rare-metal mineralization pegmatites. Pegmatites generally show lens or tabular shapes, with dominantly NW strikes, lengths less than 300 m and widths less than 5 m. The TMLT01 pegmatite is intruded into the biotite-plagioclase gneiss and hosts a small beryl-muscovite deposit (Fig. 2p). It has a length of 120 m, width of 3–5 m, strike of NNW 340° and dip angle of 65°. Four textural zones are

observed, including a coarse graphic zone (~20% vol.), blocky microcline zone (~25% vol.), quartz-muscovite zone (~45% vol.) and quartz core zone (~10% vol.). Coarse muscovite (greater than 5 cm) is mainly hosted in the quartz-muscovite zone, and beryl mineral is hosted in the graphic zone and quartz-muscovite zone (Fig. 2q), while tourmaline-(Fe) and almandine-spessartite minerals are commonly observed in most zones. According to the structure-mineral-chemistry figures (Table 1), it is denominated as a gneissic biotite granite-hosted tabular-zoned Nb-P-B-Be-muscovite-quartz-Ca-Na-K feldspar pegmatite.

3. Sampling and analytical methods

Samples QBL02, JMHB02, AMLG01 and TMLT01 were collected from the graphic texture zones of the QBL02, JMHB02, AMLG01 and TMLT01 pegmatites, respectively. Sample TLT01 was collected from the blocky microcline zone of the TLT01 pegmatite, and sample ALJK01 was collected from the bulk ALJK01 pegmatite rock.

Zircon target preparation, image acquisition under cathodoluminescence (CL), and in situ U-Pb and Hf isotope analyses were performed at the State Key Laboratory of Continental Dynamics, Northwest University, Xi'an, China. The U-Pb dating was conducted on an Agilent7500a ICP-MS instrument equipped with a 193-nm ArF excimer laser. The working conditions were as follows: laser frequency of 10 Hz with energy of 34–40 mJ, beam diameter of 30 μm, background acquisition of 30 s and signal acquisition of 60 s. Helium was used as the carrier gas to provide efficient aerosol delivery to the torch (Yuan et al., 2004). The $^{206}Pb/^{207}Pb$, $^{206}Pb/^{238}U$ and $^{207}Pb/^{235}U$ ratios were calculated by ICPMS Data Cal (Liu et al., 2009a) and were corrected using the zircon 91,500 as an external standard with a recommended $^{206}Pb/^{238}U$ age of 1065.4 ± 0.6 Ma (Wiedenbeck et al., 2004). The U, Th and Pb concentrations were calibrated using ^{29}Si as an internal standard and NIST 610 as an external standard. The concordia diagrams and weighted mean calculations were producing using the Isoplot program (Ludwing, 2003). The two standard zircons 91,500 and GJ-1 yielded weighted mean $^{206}Pb/^{238}U$ ages of 1063.7 ± 3.3 Ma (n = 24, 2σ) and 602.8 ± 3.5 Ma, respectively, which are in good agreement with the recommended ID-TIMS ages (Wiedenbeck et al., 2004). The correction of common Pb was achieved according to the method of Andersen (2002). The uncertainty of individual analyses was reported at the 1σ level, and the weighted mean $^{206}Pb/^{238}U$ age was calculated at the 2σ level.

Zircon Hf isotopic analysis was conducted on a Nu Plasma HR MC-ICP-MS equipped with a GeoLas 2005 193-nm ArF excimer laser ablation system. The analyses were performed with a spot size of 44 μm, laser repetition rate 10 Hz and energy density of 15–20 J/cm^{-2}. Helium was used as the carrier gas. The detailed instrumental settings and analytical procedures were described by Diwu et al. (2011). Zircons 91,500 and GJ-1 were also analyzed as unknown samples to check the data quality. The obtained $^{176}Hf/^{177}Hf$ ratios were 0.282305 ± 0.000028 (n = 18, 2σ) for 91,500 and 0.282036 ± 0.000017 (n = 18, 2σ) for GJ-1, which were consistent with the recommended ratios within 2σ error (0.283075 ± 0.000058 and 0.282015 ± 0.000019, respectively) (Griffin et al., 2006).

4. Results

4.1. Morphology, Th/U ratios and CL features of zircons

Sample JMHB02. Zircon grains vary in size from 80 to 120 μm; they are pale yellow in color and transparent with euhedral habit featuring {1 1 1}, {1 1 0} and {1 0 0} crystal faces. Most zircons show bright cathodoluminescence (CL) images and evident oscillatory zoning, and a few zircons show dark mantles and bright rims. Some mineral inclusions (e.g., quartz) are observed in zircons (Fig. 3a). All analytical spots show low contents of U and relatively high contents of Th, varying from 636 to 192 ppm and 522 to 99 ppm, respectively, with Th/U ratios varying from 0.837 to 0.321 (Supplementary table 1).

Sample QBL02. Zircon grains vary in size from 80 to 150 μm; they are brown to dark brown in color and opaque with euhedral habit characterized by {1 1 1} ± {1 1 0} crystal faces. Most zircons show weak but homogenous CL features without oscillatory zoning and mineral inclusions (Fig. 3b); a few zircons show irregular patchy texture characterized by local bright areas. Fifteen analytical spots from dark areas show low contents of U and relatively high contents of Th, varying from 477 to 73 ppm and 345 to 34 ppm, respectively, with Th/U ratios varying from 0.848 to 0.131. Five other spots from bright areas show significantly high contents of U and low contents of Th, varying from 3278 to 1118 ppm and 15 to 2 ppm, respectively, with Th/U ratios varying from 0.012 to 0.001 (Supplementary table 1).

Sample TLT01. Zircon grains vary in size from 60 to 100 μm; they are pale brown and translucent, with euhedral habit featuring {1 1 1} and {1 1 0} crystal faces. All zircons show no oscillatory zoning but have dark and homogenous mantles and bright rims. Very few inherited cores are observed in these zircons (Fig. 3c). All analytical spots show high contents of U and low contents of Th, varying from 3149 to 1782 ppm and 87 to 2 ppm, respectively, with Th/U ratios varying from 0.045 to 0.001 (Supplementary table 1).

Sample AMLG1401. Zircon grains vary in size from 150 to 300 μm; they are dark brown and opaque and euhedral to subhedral with {1 1 1} and {1 1 0} crystal faces. The zircons have similar CL features to the zircons from the sample TLT1401, such as no oscillatory zoning. A few zircons show blurred oscillatory zoning in their rims (Fig. 3d). Except for one spot with significantly very high U (14544 ppm) and Th (45 ppm), most zircons show relatively high contents of U and very low contents of Th, varying from 6235 to 1033 ppm and 21 to 2 ppm, respectively. The zircons have low Th/U ratios ranging from 0.001 to 0.009 (Supplementary table 1).

Sample ALJK01. Zircon grains vary in size from 50 to 100 μm; they are brown to dark brown in color and opaque and euhedral to subhedral with {1 1 1} and {1 1 0} crystal faces. Most zircons show no oscillatory zoning but weak CL features. Mineral inclusions (e.g., thorite) are observed in some zircons. The amorphous morphology of some zircons indicates that they have undergone metamictization. A few zircons show bright CL and evident oscillatory zoning (Fig. 3e). Seventeen analytical spots show high contents of U and low contents of Th, varying from 3801 to 2234 ppm and 266 to 9 ppm, respectively, with Th/U ratios varying from 0.095 to 0.003. Three other spots from zircon with oscillatory zoning have low contents of U and relatively high contents of Th, varying from 265 to 195 ppm and 149 to 85 ppm respectively, with Th/U ratios varying from 0.763 to 0.320 (Supplementary table 1).

Sample TMLT01. Zircon grains vary in size from 200 to 400 μm; they are dark brown and opaque and have euhedral habit with {1 1 1} and {1 1 0} ± {1 0 0} crystal faces. The zircons show no oscillatory zoning but weak and homogenous CL features. A few zircons show metamict features characterized by a spotted texture (Fig. 3f). The zircons have relatively high contents of U and low contents of Th, varying from 5652 to 2182 ppm and 77 to 2 ppm, respectively, with Th/U ratios varying from 0.001 to 0.019 (Supplementary table 1).

4.2. Zircon U-Pb ages and Hf isotopic compositions

Sample JMHB02. Twenty zircons with oscillatory zoning define an age population with $^{206}Pb/^{238}U$ ages varying from 402 Ma to 378 Ma and a weighted mean $^{206}Pb/^{238}U$ age of 394.8 ± 4.0 Ma (Supplementary table 1; Fig. 4a). The age of 394.8 ± 4.0 Ma represents the formation age of the pegmatite. Fifteen spots from fifteen zircon grains yield $^{176}Hf/^{177}Hf$ values ranging from 0.282668 to 0.282777. According to the crystallization time of 395 Ma, the calculated $\varepsilon_{Hf(t)}$ values range from +4.69 to +7.89 with T_{DM} model ages of 1088–885 Ma (Supplementary table 2).

Sample QBL02. A total of twenty zircons were selected for age

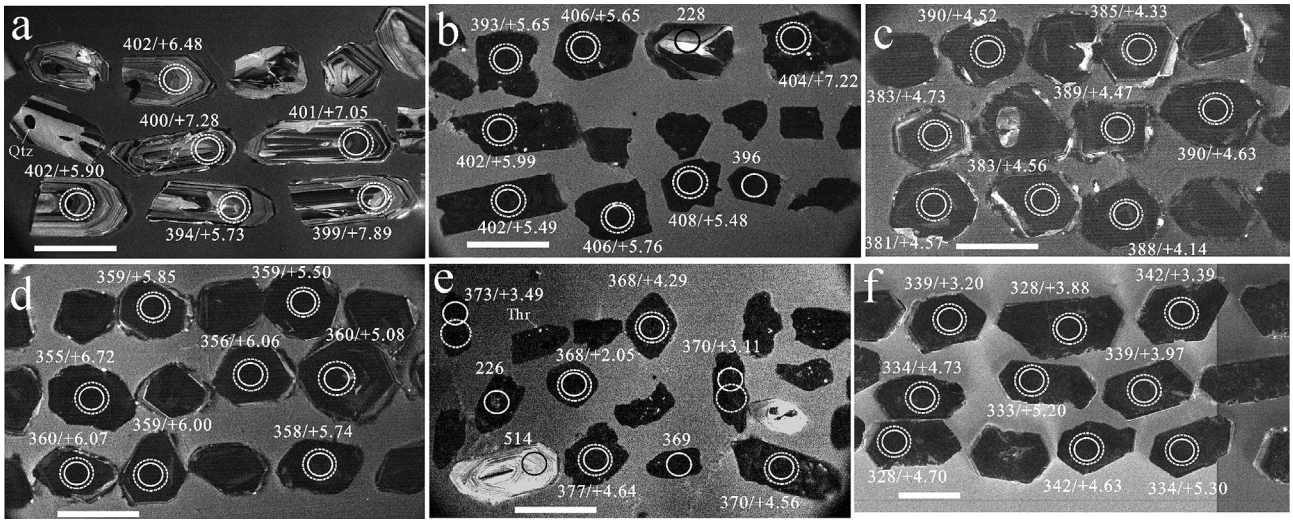

Fig. 3. Representative cathodoluminescence (CL) images of zircon, showing the laser analytic spots, mineral inclusions, $^{206}Pb/^{238}U$ ages and/or $\varepsilon_{Hf(t)}$ values. (a), (b), (c), (d), (e) and (f) show zircons from samples of JMHB02, QBL02, TLT01, AMLT01, ALJK01 and TMLT01, respectively. Scale bars correspond to 100 μm.

determination. Thirteen zircons with weak CL define a population with $^{206}Pb/^{238}U$ ages varying from 408 Ma to 393 Ma and a weighted mean $^{206}Pb/^{238}U$ age of 402.6 ± 5.5 Ma (Supplementary table 1; Fig. 4b). Two zircons with weak CL yield a younger age and an older age deviating from the concordia due to radioactive Pb loss and/or U acquisition. Five zircons with bright CL define a population with $^{206}Pb/^{238}U$ ages varying from 234 Ma to 225 Ma, which may reflect the age of recrystallization. Thus, the weighted mean $^{206}Pb/^{238}U$ age of 402.6 ± 5.5 Ma should represents the formation age of the pegmatite. Twelve spots from twelve zircon grains yield $^{176}Hf/^{177}Hf$ values ranging from 0.282609 to 0.282733; according to the crystallization time of 403 Ma, the calculated $\varepsilon_{Hf(t)}$ values range from +3.12 to +7.22 with T_{DM} model ages of 1186–934 Ma (Supplementary table 2).

Sample TLT01. Twenty analytical spots from twenty zircons with weak CL define an age population with $^{206}Pb/^{238}U$ ages varying from 390 Ma to 381 Ma and a weighted mean $^{206}Pb/^{238}U$ age of 385.9 ± 3.5 Ma (Supplementary table 1; Fig. 4c). The age of 385.9 ± 3.5 Ma represents the formation age of the pegmatite. Fifteen zircon grains yield $^{176}Hf/^{177}Hf$ values ranging from 0.282645 to 0.282676; according to the crystallization time of 386 Ma, the calculated $\varepsilon_{Hf(t)}$ values range from +3.99 to +5.06 with T_{DM} model ages of 1125–1057 Ma (Supplementary table 2).

Sample AMLG01. Twenty zircons with weak CL were selected for the age determination; four of them yield younger and discordant ages with $^{206}Pb/^{238}U$ ages varying from 328 to 133 Ma due to metamictization and radioactive Pb loss; sixteen other zircons define an age population with $^{206}Pb/^{238}U$ ages varying from 361 Ma to 355 Ma and a weighted mean $^{206}Pb/^{238}U$ age of 358.3 ± 4.6 Ma (Supplementary table 1; Fig. 4d). Twelve zircon grains yield $^{176}Hf/^{177}Hf$ values ranging from 0.282705 to 0.282756; according to the crystallization time of 358 Ma, the calculated $\varepsilon_{Hf(t)}$ values range from +5.50 to +7.28 with T_{DM} model ages of 1008–895 Ma (Supplementary table 2).

Sample ALJK01. Fourteen zircons define a population with $^{206}Pb/^{238}U$ ages varying from 373 Ma to 357 Ma and yield a weighted mean $^{206}Pb/^{238}U$ age of 368.0 ± 4.0 Ma. Four zircons yield discordant ages with $^{206}Pb/^{238}U$ ages varying from 1923 to 369 Ma due to metamictization and acquisition of common lead (Supplementary table 1; Fig. 4e). One zircon with evident oscillatory zoning yields a concordant age of 514 Ma, which indicates it is a zircon xenolith from the wall rocks. One zircon with patchy texture yields a concordant age of 226 Ma, which may represent the age of recrystallization. Thus, the weighted mean age of 368.0 ± 4.0 Ma is the formation age of the pegmatite. Fourteen zircon grains were selected for determination Hf isotopic compositions and yield consistent $^{176}Hf/^{177}Hf$ ranging from 0.282610 to 0.282697; according to the crystallization time of 368 Ma, the calculated $\varepsilon_{Hf(t)}$ values range from +2.05 to +4.64 with T_{DM} model ages of 1234–1071 Ma (Supplementary table 2).

Sample TMLT01. A total of fifteen zircons were selected for the age determination. Four of them yield discordant ages with varying $^{206}Pb/^{238}U$ ages of 795–394 Ma due to metamictization and evident acquisition of common lead. Eleven other zircons define an age population with $^{206}Pb/^{238}U$ ages varying from 342 Ma to 326 Ma with a weighted mean $^{206}Pb/^{238}U$ age of 333.0 ± 6.0 Ma (Supplementary table 1; Fig. 4f), which represents the formation age of the pegmatite. Eleven zircon grains yield $^{176}Hf/^{177}Hf$ values ranging from 0.282656 to 0.282718 (Table 2); according to the crystallization time of 333 Ma, the calculated $\varepsilon_{Hf(t)}$ values range from +3.20 to +5.20 with T_{DM} model ages of 1135–1008 Ma (Supplementary table 2).

5. Discussion

5.1. Type, age and generation of pegmatitic rocks in the Chinese Altai

Based on the rock-forming and accessory minerals, the pegmatites in the Chinese Altai have been classified into four types and nine subtypes (Zou and Xu, 1975). The subtype I, subtypes II to IV, and subtypes V to IX pegmatites have also been ascribed to the metamorphic differentiation, migmatic metasomatism and magmatic differentiation origins, respectively (Wu and Zou, 1989). However, these classification schemes are insufficient to summarize all types of pegmatite in the Chinese Altai. For example, the Liangkeshu pegmatite which is located in the northeastern of Kelang basin and intrudes into the contact zone between a monzonitic granite and biotite-quartz schist, hosts a small Fe ore deposit (Jiang, 2012). In addition, most pegmatites with no physical relation to the potential parental granite have been ascribed to the differentiation origin from granitic melts (Wu and Zou, 1989; Zou and Li, 2006). Therefore, it is need to reexamine the types of pegmatite in the Chinese Altai.

The CMS (Chemical composition-Mineral assemblage-Structural geology) classification of pegmatite (Dill, 2015a, b, 2016) is a comprehensive and practical scheme and acts as missing link between the geology and mineralogy of pegmatite. Combining this classification with previous works (Zou and Xu, 1975; Wu and Zou, 1989) and our long-term field works, the type of pegmatite in the Chinese Altai is preliminarily proposed in this work (Table 2). The five pegmatite types, including pegmatite, plutonic pegmatite, metapegmatite, pegmatoid

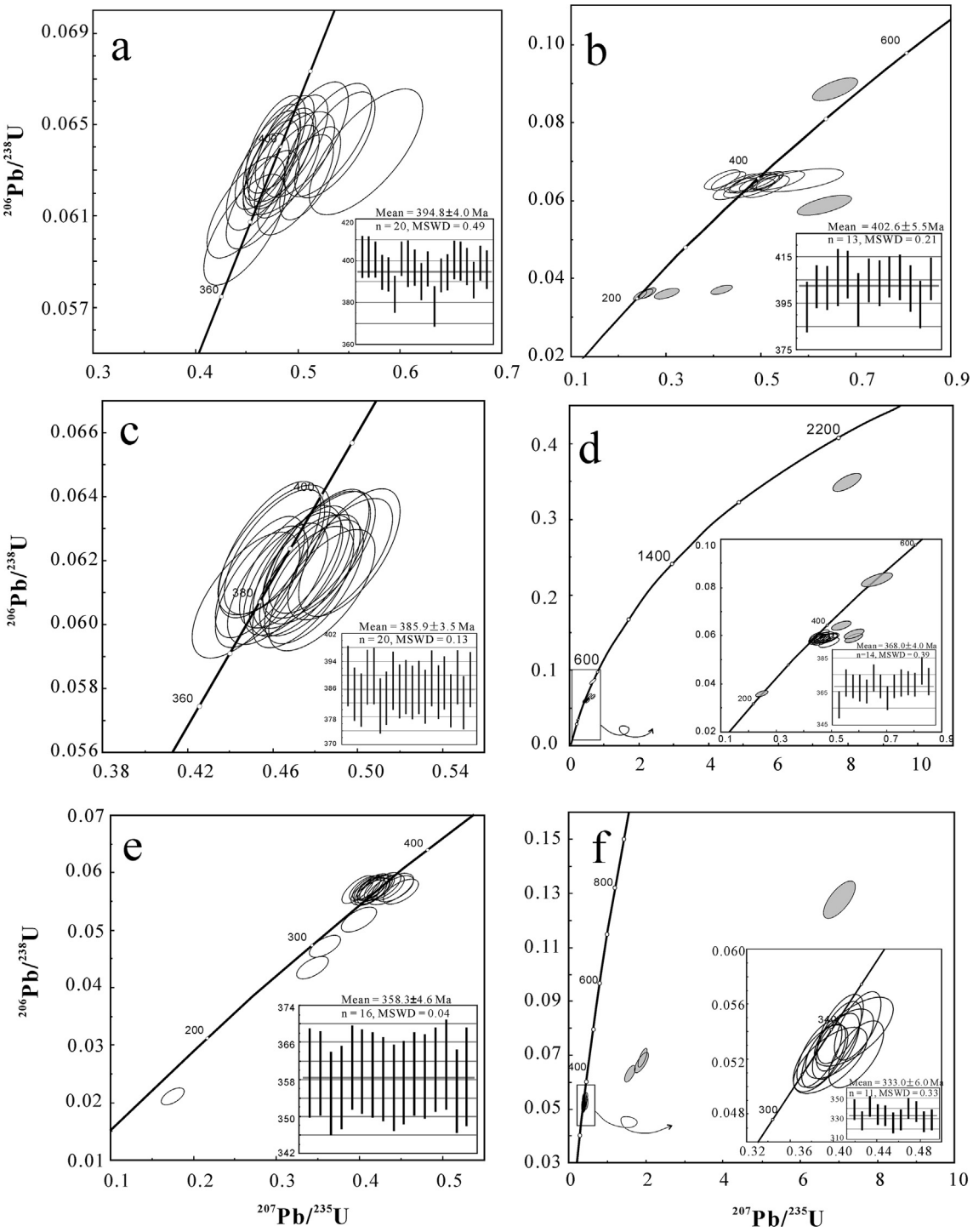

Fig. 4. Concordia and weighted average diagrams showing the LA-ICP-MS U-Pb ages of zircons from samples JMHB02 (a), QBL02 (b), TLT01 (c), ALJK01 (d), AMLG01 (e) and TMLT01 (f). Mean ages were calculated from age spot without padding gray, error ovals are 1 sigma and mean ages given as 2 sigma.

and pseudopegmatite, specified by Dill (2015a, b, 2016), can be confirmed in the Chinese Altai. Comparatively, the latter three types are less focused and studied compared with the former two due to their smaller scale and lower mineralization grade. The pegmatites with a metamorphic differentiation origin are ascribed to the mobilizate differentiated from metamorphic rocks of migmatite and gneiss, and show no zoning but equigranular texture (Wu and Zou, 1989) (Fig. 5b). Therefore, these pegmatitic rocks should belong to the pegmatoid type in the CMS classification (Dill, 2015a, b, 2016). Some of them host a few of metamorphic minerals (e.g., kyanite, and epidote), indicating a metapegmatoid type. Although there is no chronology research conducted, these pegmatoids are suggested to be formed under a prograde metamorphism with increasing temperature and pressure induced by compression during subduction process (Wu and Zou, 1989). And pegmatoids are commonly crossed by late pegmatite (Fig. 5c), indicating a synorogenic setting. Three muscovite ore deposits, including the Yelaman pegmatite from the Yeliuman-Hailiutan pegmatite field and the Baixing and Nasenqia pegmatites from the Qinghe pegmatite field have dated by Rb-Sr and Ar-Ar isochron methods at 426 ± 13 Ma, 436 ± 3.8 Ma and 448 ± 3.2 Ma, respectively. Two late tectonic-

Table 2
The CMS classification of the pegmatitic rocks from the Chinese Altai.

Geodynamic unit	Pegmatitc locations	Shape and structure	Contact relationship	Mineral association	Host rocks	Chemical qualifier	Type	Geodynamic setting	Age and reference
Qiongkuer domain	Aweitan Kuertu Tiemulete Nalinsala	Veinlet Pocket Schlieren arborization	Gradual	K-Ca feldspar, quartz, muscovite, tourmaline-(Fe), apatite-(F), magnetite, ilmenite, rutile, almandine, kyanite, epidote	migmatite, gneiss	F-B F-P-B REE-Nb-F	pegmatoid meta-pegmatoid	Synorogenic stage	? (Wu and Zou, 1989; Zou and Li, 2006)
Qiongkuer domain	Yeliuman Hailiutan Baixing Nasenqia Ayoubulake	Vein-type lens pocket	Sharp	Ca-K feldspar, muscovite, quartz, beryl, magnetite, spodumene, triphylite, sicklerite, columbite-(Fe), tourmaline-(Fe), apatite-(F), ilmenite, almandine, kyanite, epidote, andalusite, euxenite, samarskite, xenotime-(Y)	schist, gneiss	F-P-B Be-P-B Nb-B-Be Nb-REE-F-Li-Be	meta- pegmatite	preorogenic stage	476–426 Ma (Wang et al., 2001; Ren et al., 2011)
Qiongkuer and Central Altai domains	Amulagong Talati Qiebielin Jiamanhaba Alajieke Tiemulete	Tabular stock-like vein-type	Sharp	(Ca)-Na-K feldspar, quartz, muscovite, beryl, spodumene, columnite-(Fe), columbite-(Mn), tantalite-(Mn), hydroxymanganopyrochlore, hluorcalciomicrolite, trilithionite, polylithionite, lithiophilite, pollucite, bismutite, amblygonite, apatite-(Mn), spessartine, tourmaline-(Fe), zircon, hafnian zircon, gahnite	schist, gneiss, gneissic granite, metabasite	P-B P-Li P-B-Be P-B-Nb-Be Bi-P-B-Nb/Ta-Be-Li Bi-P-B-Cs-Nb/Ta-Be-Li	pegmatite	Forearc extensional setting during subduction	403–330 Ma (this work)
	BieyesamasiKoktokay Alaer Kujierte Kuwei Kelumute Jideke Azubai Kaluan Husite Hulugong Bazhai Dakalasu Xiaokalasu					Bi-P-B-Hf-Rb-Cs-Nb/Ta-Be-Li		Attenuation of the thickened crust during postorogenic stage	230–180 Ma (Wang et al., 2007; Ren et al., 2011; Lv et al., 2012, 2015; Ma et al., 2015; Zhang et al., 2016; Zhou et al., 2016)
Qiongkuer domain	Saerjiake Taerlang Wulukete Qiemuerqieke Kekexier	Vein-type lens tabular	Sharp	Ca-Na-K feldspar, quartz, muscovite, beryl, spodumene, lepidolite, columbite-(Fe) and -(Mn), euxenite, samarskite, fergusonite, xenotime-(Y), monazite-(Ce), columbite, ilmenorutile-(Nb), magnetite, almandine-spessartite, fluorite, tourmaline-(Fe), apatite-(Mn), zircon	schist, gneiss, gneissic granite	F-B F-Be-B Be-P-B (F)-REE-P-B Nb-REE-F-Be-P-B Nb/Ta-P-B-Be-Li	pegmatite	Arc-continent collision and thickening of the crust; Attenuation of the thickened crust during postorogenic stage	280–250 Ma and 250–230 Ma (Ren et al., 2011; Zhou et al., 2016; unpublished data)
Qiongkuer domain	Shangkelan	Vein-type	Gradual	Na-K feldspar, quartz, muscovite, wolframite, fluorite, monazite-(Ce), xenotime-(Y), columbite-(Fe), zircon, thorite, ilmenorutile -(Nb), bismutite	Greisen or muscovite -albite granite	F-Th-Bi-REE-Nb-W-Be	Granitic pegmatite	Deep fault zone during postorogenic	193–175 Ma (Wang et al., 2002)
Kelang basin Qiongkuer domain	Liangkeshu	Lens	Sharp	Ca-K feldspar, quartz, muscovite, magnetite, pyrite, almandine, pyrope, epidote	quartz-biotite schist and monzonitic granite	Mn-Mg-Fe	Pseudo-pegmatite	Forearc extensional basin during subduction	376-? Ma (Jiang, 2012)

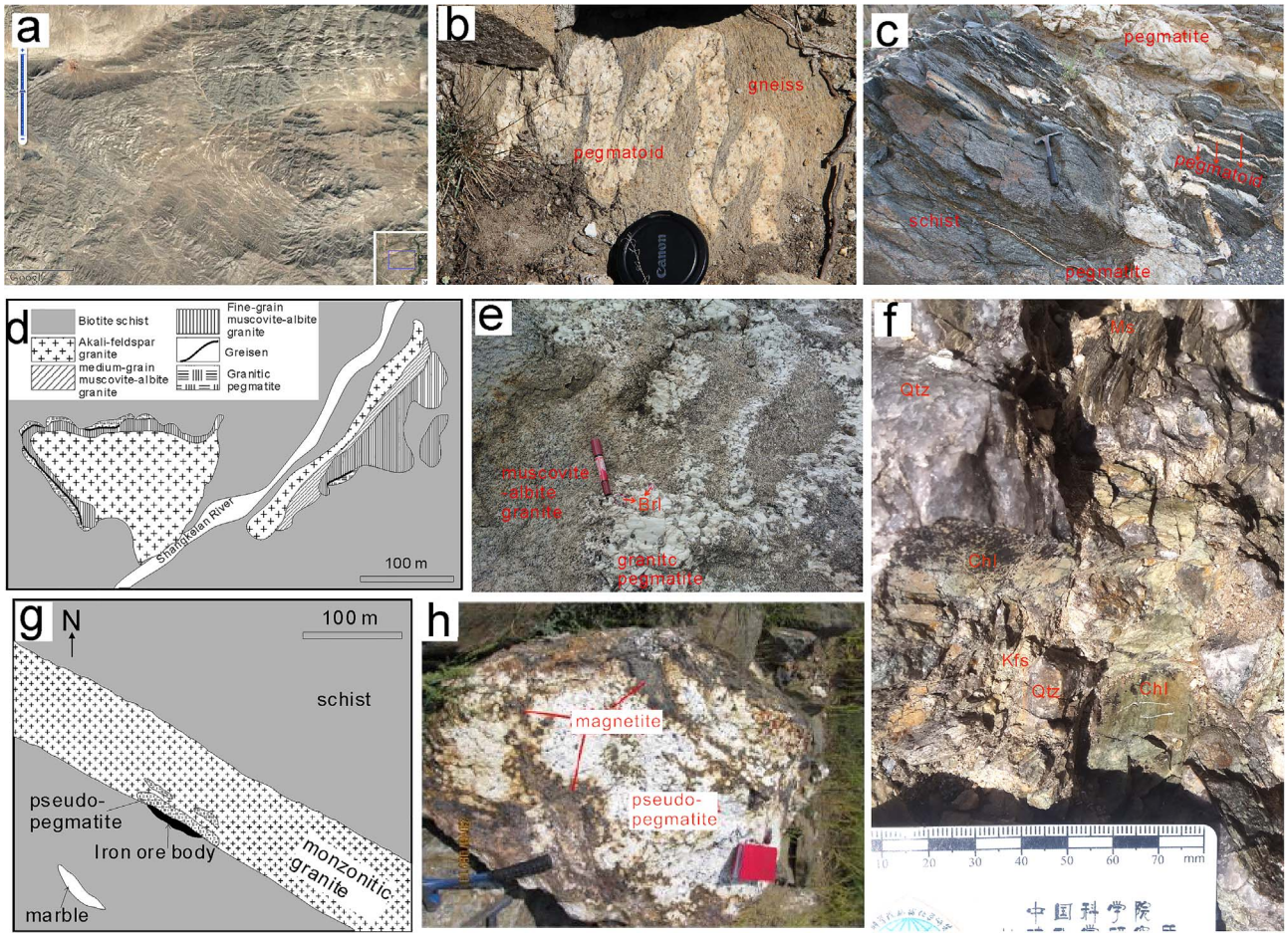

Fig. 5. The satellite, field and geological maps of pegmatitic rocks from the Chinese Altai. (a) shows that the emplacement of pegmatite is controlled by anticline structure in the Alajieke area; (b) the pegmatoid with corrugation structure hosted by gneiss in the Tiemulete area; (c) the pegmatoids crossed by late pegmatite in the Tiemulete area; (d) the geological map of Shangkelan granites, greisen and granitic pegmatite (according to Zou and Li, 2006); (e) the local contact between fine-grain muscovite-albite granite and granitic pegmatite; (f) the local mineral assemblage of Yeliuman metapegmatite; (g) the geological map and (h) the disseminated magnetites of Liangkeshu pseudopegmatite (according to Jiang, 2012).

thermal events at ca. 380 Ma and 240 Ma are reflected by their Ar-Ar plateau age. In addition, lots of kyanite has also been observed (Wang et al., 2001). The oldest pegmatite so far from Yeliuman is dated by zircon U-Pb at 476 ± 12 Ma (Ren et al., 2011). It is cut by a late shear failure which induces evident epidotization and muscovitization (Fig. 5f). These pegmatites should be classified as a metapegmatite type (Table 1). The iron ore deposits in Liangkeshu pegmatite has been interpreted as a differentiated production from the pegmatite-forming melt. The iron ore body shows a lens shape sandwiched by the pegmatite and schist, and is half the size of the pegmatite (Fig. 5 g) (Jiang, 2012). It is hard to believe that such large iron ore body comes from a felsic dike. Actually, many iron ore deposits are formed in Kelang basin (Yang et al., 2013), and the Liangkeshu pegmatite is located very close to the Jiaerbasidao Fe deposit (286 Ma, Yang et al., 2013). The skarnization and magnetite disseminated structure (Fig. 5 h) in the footwall of Liangkeshu pegmatite (~376 Ma, Jiang, 2012) probably result from the overprint by Jiaerbasidao skarn-type iron mineralization. The Liangkeshu pegmatite is a special example for the pseudopegmatite type in the Chinese Altai (Table 1). The typical pseudopegmatite characterized by an early pegmatite reworked by a late pegmatite-forming melt (Dill, 2016) also exists in the Chinese Altai, but it is always omitted and needs to be confirmed in future. The typical plutonic pegmatite derived from granite melt in the Chinese Altai is only observed in Shangkelan. According to the description by Zou and Li, 2006, an integral evolution sequence consists of coarse-grained muscovite alkali granite, medium-grained muscovite albite granite, fine-grained muscovite albite granite, greisen and pegmatite (Fig. 5d), and the gradual contact between muscovite albite granite and pegmatite (Fig. 5e) can be observed in field. The granite-pegmatite suite is formed in the early Jurassic (194–175 Ma; Zou and Li, 2006). Similar pegmatite is rarely observed in the Chinese Altai.

Compare to the four types mentioned above, pegmatites are abundant and widely distribute in the Qiongkuer and Central Altai domains (Fig. 1). They are evidently controlled by regional anticline (Fig. 5a), and commonly intrude into schist, gneiss, gneissic granite and metabasite with a sharp contact, and show vein-type, tabular, stock-like and lens shapes (Table 2). The large temporal gaps commonly observed between these pegmatites and the adjacent granites (Fig. 6). However, pegmatites in the Qiongkuer and Central Altai domains have distinct formation ages and mineralization types (Table 2). The former is mainly featured by Be-Nb/Ta-REE mineralization (Fig. 7), and formed in the middle Permian and Triassic (270–230) (Ren et al., 2011; Qin et al., 2013; Zhou et al., 2016; Liu et al., 2017; Our unpublished data). The latter is featured by Be-Li-Nb/Ta-Cs mineralization (Fig. 7), and formed in the middle Triassic and early Jurassic (230–180 Ma) (Zhu et al., 2006; Wang et al., 2007; Ren et al., 2011; Lv et al., 2012, 2015; Qin et al., 2013; Liu et al., 2014; Ma et al., 2015; Liu, 2015; Zhang et al., 2016; Zhou et al., 2016). The discrepancies can be ascribed to the distinct crust components of the Qiongkuer and Central Altai domains and transformations of the components during orogenic process. The Nd-Sr isotopic mapping of granites (Wang et al., 2009) and feldspar P content statistics of pegmatites (Lv et al., 2018) in the Chinese Altai indicate that the Qiongkuer domain has more juvenile crust components than the Central Altai domain.

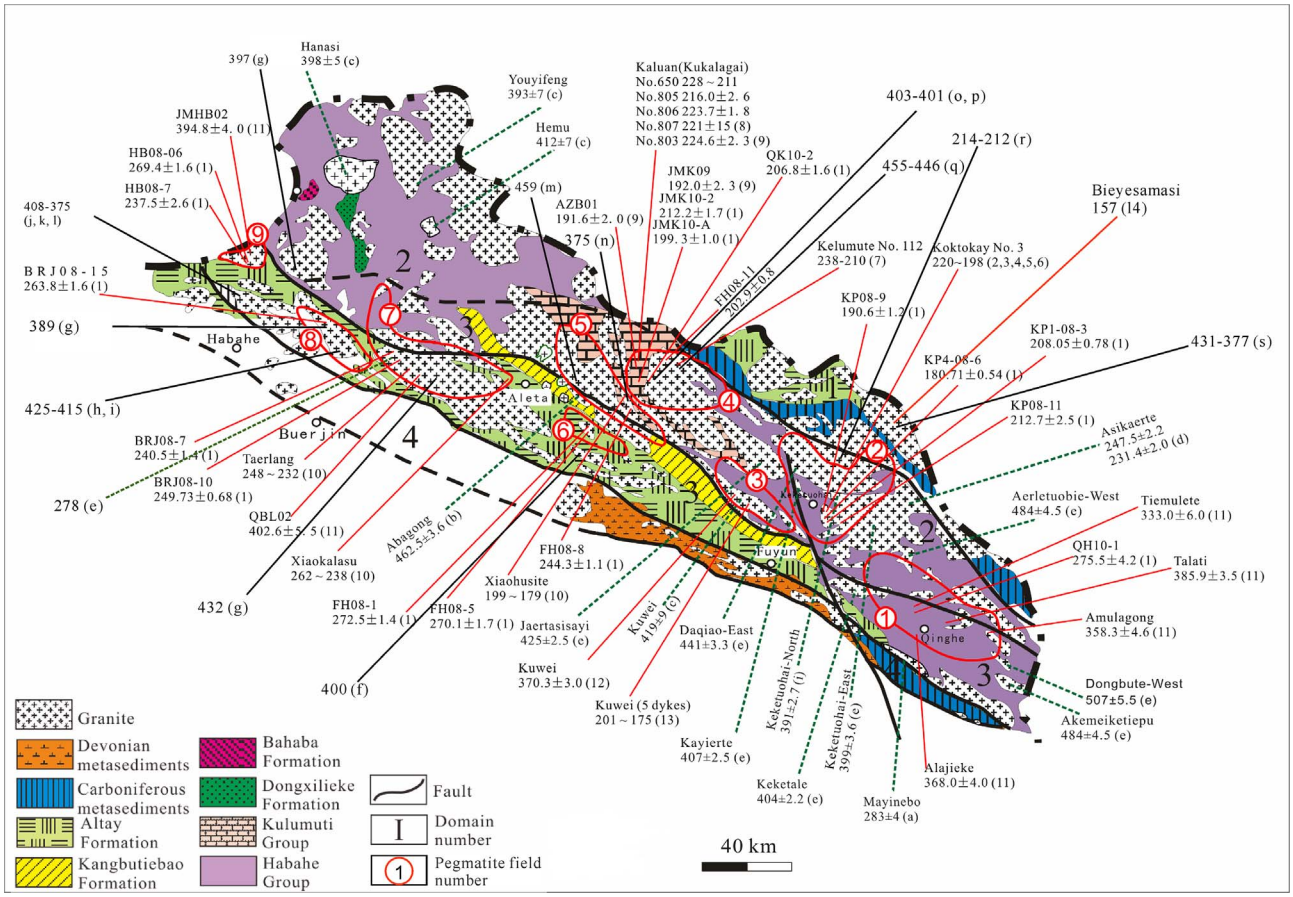

Fig. 6. Geological sketch map of the Chinese Altai shows the locations and ages of pegmatites and the neighboring I- and S-type granites. Red and black solid lines show the locations of pegmatite and I-type granite; green dotted line shows the location of S-type granite. Pegmatite data from (1) Wang et al., 2002; (2) Ren et al., 2011; (3) Zhu et al., 2006; (4) Wang et al., 2007; (5) Chen, 2011; (6) Liu et al., 2014; (7) Che et al., 2015; (8) Lv et al., 2012; (9) Ma et al., 2015; (10) Zhang et al., 2016; (11) Zhou et al., 2016; (12) this work; (13) our unpublished data and (14) Lv et al., 2015. S-type granite data from (a) Zhou et al., 2007; (b) Liu et al., 2010; (c) Cai et al., 2011b; (d) Zhang et al., 2017a,b and (e) Li et al., 2012b. I-type granite data from (f) Liu et al., 2009b; (g) Cai et al., 2011b; (h) Sun et al., 2009; (i) Sun et al., 2008; (j) Song et al., 2010; (k) Yang et al., 2014; (l) Wan et al., 2011; (m) Chai et al., 2010; (n) Wang et al., 2006; (o) Ma et al., 2015; (p) Zhang et al., 2016a; (q) Lv et al., 2012; (r) Wang et al., 2014a; (s) Lv et al., 2015. (For interpretation of the references to color in this figure legend, the reader is referred to the web version of this article.) (For interpretation of the references to color in this figure legend, the reader is referred to the web version of this article.)

According to the statistics on age and location of pegmatites in the Chinese Altai, the pegmatites formed from the Devonian to the Jurassic with a peak in the Triassic (Wang et al., 2000, 2002, 2003; Zhu et al., 2006; Wang et al., 2007; Ren et al., 2011; Lv et al., 2012, 2015; Qin et al., 2013; Liu et al., 2014; Ma et al., 2015; Liu, 2015; Zhang et al., 2016; Zhou et al., 2016), and there is more than one generation of pegmatites exposed in the same pegmatite field (Figs. 6 and 7). In the Jiamanhaba, Xiaokalasu-Qiebieling and Dakalasu-Kekexier pegmatite fields, Permian (270–260 Ma) and Triassic (250–230 Ma) pegmatites have been confirmed (Ren et al., 2011; Zhou et al., 2016). In the Kalaeerqisi, Kelumute-Jideke and Keketuohai pegmatite fields, at least two generations of pegmatites exist, including Triassic (244–203 Ma) and Jurassic (199–179 Ma) ones; (Zhu et al., 2006; Wang et al., 2007; Ren et al., 2011; Lv et al., 2012; Ma et al., 2015; Zhang et al., 2016; Zhou et al., 2016). In the Hailiutan-Yeliuman pegmatite field, Permian (264 Ma) pegmatite is also established (Ren et al., 2011). In the Kuwei-Jiebiete field, Devonian (370 Ma, Wang et al., 2002) and Early Jurassic (201–175 Ma, unpublished data) pegmatites are verified. In the Qinghe pegmatite field, Permian (297–265 Ma, Ren et al., 2011; Zhou et al., 2016) pegmatite is also confirmed. According to the chemistry-mineral-structure features (See 2.2 and Table 1), the studied pegmatites in this work belong to the pegmatite type in the CMS classification (Dill, 2015a, b, 2016). The investigated pegmatites in this work, including the JMHB02 pegmatite from the Jiamanhaba field, the QBL02 pegmatite from the Xiaokalasu-Qiebielin field and the TLT01, ALJK01, AMLG01 and TMLT01 pegmatites from the Qinghe field have zircon U-Pb ages of 394.8 ± 4.0 Ma, 402.6 ± 5.5 Ma, 385.9 ± 3.5 Ma, 368.0 ± 4.0, 358.3 ± 4.6 Ma and 333.0 ± 6.0 Ma, respectively (Fig. 4). The Talati pegmatite (TLT01) has been dated by muscovite Ar-Ar at 286.4 ± 1.6 Ma (Zhou et al., 2016). However, this age is dubious due to high temperature metamorphism at 281 ± 3 Ma in south-western Qinghe (Hu, 2006). Therefore, our age data complement the generations of pegmatite in the Chinese Altai, and this work presents the first identification of synorogenic rare metal pegmatites in the Chinese Altai.

5.2. Metamorphism and pegmatite

Para-metamorphic rocks are prevalent in the Chinese Altai and have been extensively studied in recent years. They commonly vary from greenschist- to amphibolite-facies and rarely extend up to ultrahigh-temperature (UHT) granulite facies (Windley et al., 2002; Chen et al., 2006; Hu, 2006; Briggs et al., 2007, 2009; Zheng et al., 2007; Jiang et al., 2010; Li et al., 2010, 2014). Two metamorphic peaks are characterized by UHT granulite facies at 377–391 Ma (Zheng et al., 2007; Jiang et al., 2010) and 270–290 Ma (Briggs et al., 2007, 2009; Chen et al., 2006; Hu, 2006; Li et al., 2014). They are attributed to upwelling of the asthenosphere induced by ridge subduction at approximately 390 Ma (Jiang et al., 2010) and extensional decompression induced by sinistral strike-slip along the Irtish tectonic belt and slab detachment at approximately 277 Ma (Li et al., 2014). The ultrahigh-temperature metamorphism during the subduction process ca. 390 Ma is suggested

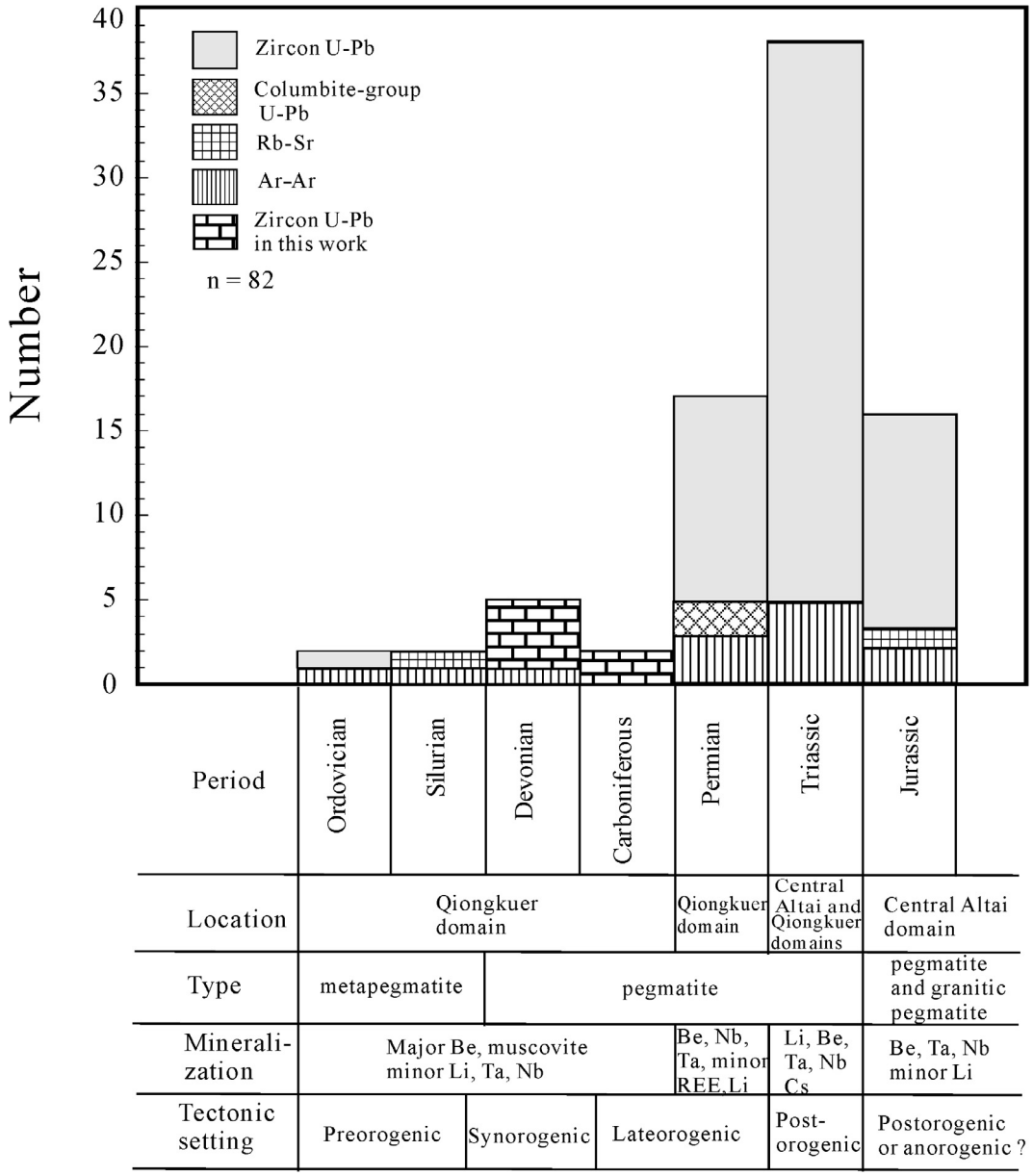

Fig. 7. Histogram for the age distribution, location, mineralization and tectonic setting of pegmatitic rocks from the Chinese Altai. Data from Wang et al., 2000, 2001, 2002, 2003; Zou and Li, 2006; Wang et al., 2007; Ren et al., 2011; Lv et al., 2012, 2015; Qin et al., 2013; Liu, 2015; Ma et al., 2015; Zhang et al., 2016; Zhou et al., 2016; Liu et al., 2017; this work and our unpublished data.

to have occurred at temperatures of 650–720 °C estimated using the amphibole-plagioclase-quartz, garnet-biotite and Ti-in-zircon geothermometers (Jiang et al., 2010). Wu and Zou (1989) have suggested that high-temperature metamorphism may activate components of H_2O, Ca, K, Na, Si, CO_2 and F in volcanic rocks and sediments by metasomatism and recrystallization. These activated components are mobilized along the decreasing *P-T* gradient and concentrated in cleavages or fissures of the parental rock, giving rise to the formation of the metamorphogenetic pegmatitic rock, i.e., pegmatoid.

Metamorphism is directly responsible for the formations of pegmatoid and metapegmatite, but not for pegmatite (Dill, 2016). Rare metal pegmatites are commonly observed in low-pressure sequences of the upper-greenschist to lower amphibolite facies, and occasionally in the andalusite-cordierite and sillimanite-bearing subfacies (Cerný, 1991a). In the Qiongkuer and Central Altai domains, the kyanite(andalusite)-staurolite and sillimanite-cordierite zones are widely developed (Zhuang, 1994), indicating the lower to upper amphibolite facies. The formation of pegmatite commonly relate to the transformation of crustal components during metamorphic-magmatic processes (Dill, 2016), and most rare metal pegmatites worldwide are formed at the late- to postorogenic stages (Cerný, 1991a; McCauly and Bradley, 2014; Bradley and McCauly, 2016; Dill, 2015a, b, 2016) which postdate the peak of regional dynamo-thermal metamorphism. The metamorphism happened in the middle-lower crust during orogenic process may contribute to the mobilization and enrichment of rare metal elements. As proposed by several authors, the granulite-facies metamorphism in the lower crust could induce the abnormal enrichment of fluxing elements (Li, F, B, Be) and HFSE (mainly Nb and Ta) (Marignac and Cuney, 1999; Cuney et al., 2002). In the Chinese Altai, the middle Paleozoic rare metal pegmatites (403–333 Ma, this work) are formed during or late to the UHT metamorphism at ca. 390 Ma (Jiang et al., 2010), and the prime rare metal pegmatites formed in Permain-Triassic (270–200 Ma, Zhu et al., 2006; Wang et al., 2007; Ren et al., 2011; Lv et al., 2012; Qin et al., 2013; Liu et al., 2014; Ma et al., 2015; Liu, 2015; Zhang et al., 2016; Zhou et al., 2016; Liu et al., 2017) are posterior to the UHT metamorphism at ca. 277 Ma (Li et al., 2014).

5.3. Relationship between the pegmatites and granites

Granitoids are widely exposed and occupy approximately 40% of the area of the Chinese Altai, indicating that magmatism contributed a large proportion to building up the Chinese Altai (Wu and Zou, 1989). They consist of ca. 200 plutons varying in composition mainly from calc-alkaline to the alkaline and peralkaline series (Jahn et al., 2000). The ages of the granites range from 510 Ma to 150 Ma and are mainly concentrated in the middle Paleozoic with a peak in the early Devonian (ca. 400 Ma) (Zhao et al., 1993; Chen and Jahn, 2002; Windley et al., 2002; Briggs et al., 2007; Wang et al., 2006, 2009, 2014a; Yuan et al., 2007; Zhou et al., 2007; Sun et al., 2008, 2009; Cai et al., 2011a, b; 2012a,b, 2016; Tong, 2006; Tong et al., 2006a, b, 2007; 2012, 2014; Wang et al., 2011; Ma et al., 2015; Zhang et al., 2017b; Yu et al., 2017). The granitoids that formed during the early-middle Paleozoic (480–330 Ma) subduction process are mostly assigned to the I-type by chronology, petrogeochemistry and isotopes and are widely exposed in the North Altai, the Central Altai and the Qiongkuer domains (Zhao et al., 1993; Yuan et al., 2001; Chen and Jahn, 2002; Tong, 2006; Wang et al., 2006, 2009; Yuan et al., 2007; Sun et al., 2008, 2009; Yang et al., 2010; Cai et al., 2011b; Lv et al., 2012, 2015; Liu, 2015; Ma et al., 2015; Zhang et al., 2016; Yu et al., 2017). In comparison, S-type granites mainly formed in the early-middle Paleozoic (507–340 Ma) with smaller numbers and limited exposures in the Central Altai domain (Liu et al., 2009b; Cai et al., 2011a; Zhang et al., 2017b). In addition, three young (283–231 Ma) and small S-type granites are confirmed as distributed in the southeastern Chinese Altai (Zhou et al., 2007; Liu, 2015) (Fig. 6). A-type granites mainly formed in the late Paleozoic (290–265 Ma) and are linearly distributed in the Qiongkuer domain (Tong et al., 2014; Liu et al., 2017). Several older (382–327 Ma) A-type granites are also verified, distributed in the southeastern Erqis domain (Tong et al., 2006a, b, 2012; Shen et al., 2011). A few granitic plutons, however, show a mixture of the features of I-type and A-type with ages ranging from 280 Ma to 200 Ma, distributed in the contiguous areas of the Abagong fault (e.g., the Lamazhao and Shangkelan granites) and the dissected areas between the Nuoerte fault and the Kalaxianger fault (e.g., the Aral batholith) (Wang et al., 2005, 2014a; Tong, 2006). According to the zircon ages and Hf isotopes of granites from the Chinese Altai, most Paleozoic S- and I-type granites have similar ages and Hf isotopes, and only a few S- and I-type granites contain evident ancient and juvenile components, respectively (Fig. 8). The S-type granites are ascribed to dehydration melting of newly accreted metasediments (e.g., the Habahe Group) induced by involvement of a mantle-derived component (Cai et al., 2011a) or partial melting of oceanic sediments and the associated mantle wedge (Zhang et al., 2017b) during subduction processes in an active margin. In contrast, the I-type granites are suggested to originate from the partial melting of the mid-crust induced by the upwelling of asthenosphere in a setting of back-arc spreading (Wang et al., 2006, 2009) or ridge subduction (Windley et al., 2007; Sun et al., 2008, 2009; Cai et al., 2011b, 2012). However, the latest work suggests that the regional anatexis of fertile sediments (the Habahe group) could generate most of the (greater than 80%) Silurian-Devonian granites in the Chinese Altai (Jiang et al., 2016), indicating the significance of anatexis in the formation of granitic magma in this region.

As stressed by Dill (2015a,b), the temporal relation between pegmatites and neighboring granites plays a key role to distinguish the origin of pegmatites. In the Central Altai domain, pegmatites are intensively formed in the middle Triassic to early Jurassic (230–180 Ma), postdate the formations of the early-middle Paleozoic I-type (480–330 Ma) and S-type (507–340 Ma) granites and also the rare Permian-Triassic S-type granites (283–231 Ma). In the Qiongkuer domain, the early-middle Paleozoic I-type (480–330 Ma) and late Paleozoic A-type granites (290–265 Ma) are widely formed, but pegmatites are mainly formed in the middle Permian-Triassic periods (270–230 Ma). The studied pegmatites in this work show zircon U-Pb ages of 403–333 Ma, temporally and partly overlap with the early-middle Paleozoic I-type granites (480–330 Ma) but separate from each other in space (Fig. 6). As mentioned above (see 2.2), the Jiamanhabe pegmatite field is occupied by the Caledonian biotite granite and plagiogranite and the late Variscan two-mica granite (Zou and Li, 2006), but the JMHB02 pegmatite is formed at ca. 395 Ma (Fig. 4a). The biotite granite and two-mica granite exposed in the Qiebielin pegmatite field are dated at 432 ± 7 Ma (Cai et al., 2011b) and 278.6 ± 3.5 Ma (Li et al., 2012b) by zircon U-Pb, respectively. However, the QBL02 pegmatite intrudes into the biotite granite at ca. 403 Ma (Fig. 4b). In the Qinghe pegmatite field, the early Variscan diorite and middle Variscan porphyritic biotite granite are exposed in the Amulagong mining area. Other S-type granites exposed in adjacent areas (Fig. 5), such as the Keketale, Aerletuobie and Dongbute granites, have older intrusive ages (507–404 Ma, Zhang et al., 2017b) than the studied pegmatites (386–333 Ma, Fig. 4c, d, e and f) (Fig. 6).

The large temporal gaps between pegmatites and neighboring granites are widely observed in the Chinese Altai. In the Koktokay pegmatite field, rare metal pegmatites are formed at 220–180 Ma (Zhu et al., 2006; Wang et al., 2007; Ren et al., 2011), but the granites at there are proved to be older intrusions (441–391 Ma; Wang et al., 2006; Cai et al., 2011b; Zheng et al., 2016; Song et al., 2010; Zhang et al., 2017b). The Aral biotite granite, tens kilometers away from the Koktokay No. 3 pegmatite, has been ascribed to the parental rock of the pegmatite due to similar ages and Hf and Nd isotopes (Zhu et al., 2006; Liu et al., 2014). However, it is precluded from being fertile granite due to its high K/Rb ratios (246–167) and low abundances of Rb (656–454 ppm) and Cs (6.26–2.42 ppm) in K-feldspars. Further, according to calculations based on the Rayleigh fractionation model, the Aral granite would be required to undergo 99.999% fractional crystallization to yield the No. 3 pegmatite (Liu, 2013), which is impossible. In the Bieyesamasi mining area, the No. L1 rare metal pegmatite (157 Ma) and the neighboring coarse- and fine-grained two-mica granites (431 Ma and 377 Ma, respectively) show distinct zircon U-Pb ages (Lv et al., 2015). In the Kelumute-Jideke pegmatite field, the late Ordovician biotite granite (455 Ma) and gneissic two-mica granite (446 Ma) are widely exposed in the Kelumute mining area and host the Triassic pegmatites (238–203 Ma, Ren et al., 2011; Lv et al., 2012). The Kaluan Li-rich pegmatites (228–211 Ma, Ma et al., 2015) and Azubai Be-rich pegmatites (215–192 Ma, Zhang et al., 2016; unpublished data) intruded into the Silurian schists, and have been ascribed to the differentiation products of the Halong biotite granite and two-mica granite located in the eastern of the Kaluan-Azubai mining area. However, these granites are dated by zircon U-Pb at 403–401 Ma (Ma et al., 2015; Zhang et al., 2016) (Fig. 6).

Not only that, the temporal gap between granites and pegmatites is also widely observed in worldwide. Base on the large temporal gaps between the different generations' pegmatites and neighboring granites in the CAOB, Zagorsky et al., (2014) claim the necessity for recognition of an independent pegmatite stage in collision and continental-rift settings. In the Hagendorf-Pleystein pegmatite Province, Central Europe, abundant pegmatites also show distinct temporal gap to granites exposed in the same areas. Besides that, the supposed 'deep parental granite' is excluded by geophysical survey and rock samples from boreholes. Base on the rounded analysis of the distribution of elements Li, Be, B, P, Zn, As, Bi, Nb, Ta, Ba, Rb, REEs, Th and U in granites, pegmatites and metamorphic rocks, the element cycling models are established (Dill, 2015a). It is no doubt that the works on the Hagendorf-Pleystein pegmatite Province set the example for pegmatite study, and significantly contribute to the pegmatite science.

Compared with the Paleozoic I- and S-type granites in the Chinese Altai, the pegmatites in this work show a narrow $\varepsilon_{Hf}(t)$ range of +8.28–+2.06 and T_{DM2} ages ranging from 840 to 1230 Ma, which overlap with those of the most I- and S-type granites (Fig. 8), indicating that the pegmatites and most granites in the Chinese Altai have a similar source from an immature crust. As mentioned above (see 2.1), the Chinese Altai is a Paleozoic magmatic arc and mainly consist of the

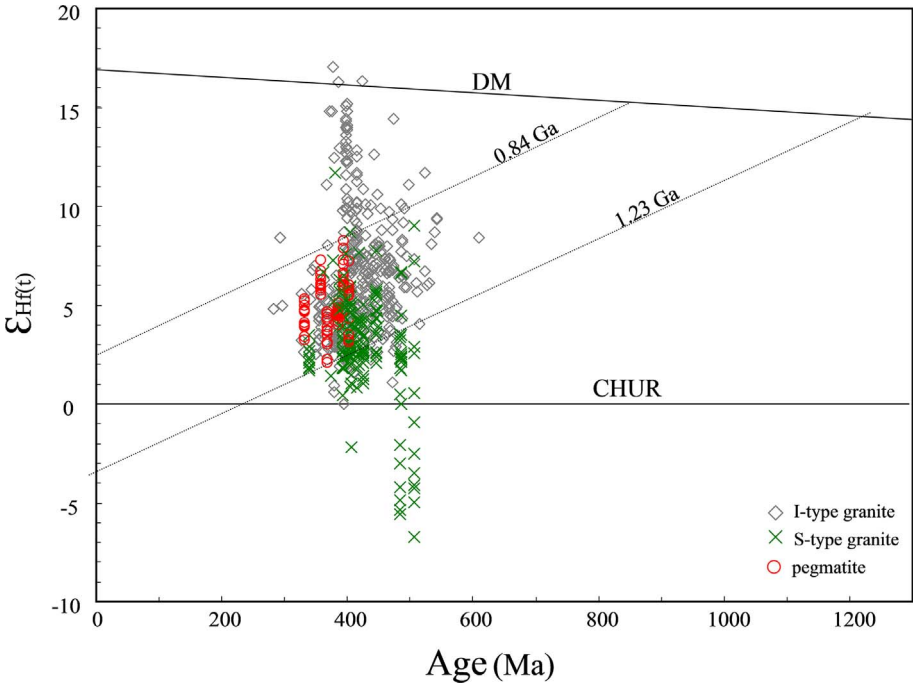

Fig. 8. Diagram of εHf(t) values versus crystallizing ages for zircons from the early-middle I- and S-type granites and pegmatites in the Chinese Altai. DM = depleted mantle, CHUR = chondrite uniform reservoir. Granite data from Sun et al., 2008, 2009; Cai et al., 2011a, b; Ma et al., 2015; Yu et al., 2017; Zhang et al., 2017a,b. Pegmatite data from this work.

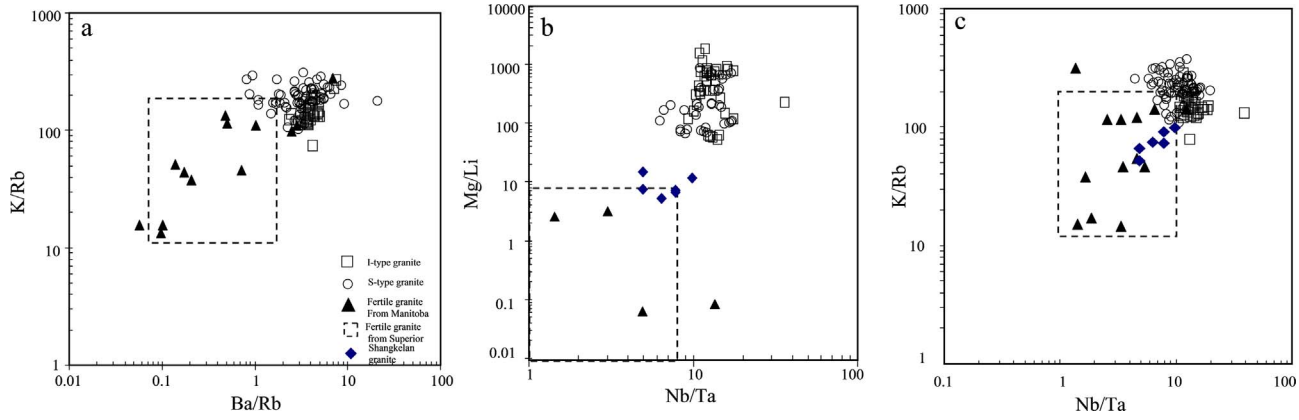

Fig. 9. The distribution of K/Rb versus Ba/Rb (a), Nb/Ta (b), and Mg/Li versus Nb/Ta (c) of the Paleozoic I-type granites from the Qiongkuer domain and S-type granites from the Chinese Altai. Compare to the ratios of the typical fertile granites from Superior and Manitoba, Canada and the Shangkelan granites, the granites from the Chinese Altai show low fractionation grade. Data of the granites from the Chinese Altai refers to Wang et al., 2006; Yuan et al., 2007; Sun et al., 2008; Cai et al., 2011a; Zhang et al., 2017a,b; data of the Shangkelan granites from Zou and Li, 2006; data of the fertile granites from Canada refers to Selway et al., 2005; Černý et al., 2012b.

Paleozoic volcanic-sedimentary formations and the Paleozoic-Mesozoic igneous rocks. And the geophysical study (Wang et al., 2003a,b) and petrographic studies do not support a Precambrian basement in the Chinese Altai (Long et al., 2007, 2008, 2010, 2012; Liu et al., 2012; Jiang et al., 2011, 2016; Cai et al., 2011a,b; 2012a,b; Wang et al., 2014b; Yu et al., 2017). Thus, it is not surprising that these synchronous granites and pegmatites have similar Hf isotope compositions. These granites are separated from the studied pegmatites in location. And compared with the typical fertile granites (parental granites of pegmatites) from Superior and Manitoba, Canada (Selway et al., 2005; Cerný et al., 2012b) and the Shangkelan granite sequence mentioned above (Zou and Li, 2006), the Paleozoic I-type granites from the Qiongkuer domain and S-type granites from the Chinese Altai (Wang et al., 2006; Yuan et al., 2007; Sun et al., 2008; Cai et al., 2011a; Zhang et al., 2017b) commonly show ratios of Mg/Li, K/Rb, Ba/Rb and Nb/Ta distinct from those of fertile granites (Fig. 9a, b and c), indicating that they are less fractionated and belong to barren granite. As proved by the studies on granites and pegmatites from the Hagendorf-Pleystein pegmatite Province, the relationship between these two rocks is more like brother and sister (Dill, 2015a).

Granite plays a key role in formation of the granitic pegmatite, and it is the essential difference between granitic pegmatite and pegmatite. For the former, the differentiation sequence from parental granite to transition facies and to final pegmatite can be observed in field. In addition, the rare metal mineralization in granitic pegmatite mainly relates to Sn, W, Be, U, F and Li, especially Sn and W (Dill, 2015a, b). The Sn-W ore deposits associated with granite and its differentiated rocks is prevalent worldwidely, but similar ore deposits with industrial grade is rarely developed in pegmatite. The Greenbush Sn-Ta-Li-Nb 'pegmatite' is known as a large pegmatite-type Sn ore deposits. However, it is proved to be reworked by two late deformation-metamorphic events (Partington et al., 1995), and should belong to the pseudo-pegmatite type according to the CMS classification (Dill, 2015b). The superlarge granite-type W-Sn ore deposits are prevalent in southern China, but the industrial grade Li-Be-Ta-Nb-mineralized pegmatite is absent. In the Chinese Altai, W- and Sn-ore forming minerals are

commonly absent in pegmatite and both elements are only incorporated as trace element in some accessory minerals, but the wolframite mineral is abundant in the Shangkelan granitic pegmatite (Zou and Li, 2006). By contrast, granite-type W mineralizations are prevalent in the Russia Altai (Vladimirov et al., 1998) with formation ages in the late Triassic to late Jurassic (Annikova et al., 2006; Han, 2008), postdate the Permian-Triassic rare pegmatites in the Chinese Altai. In the Hagendorf-Pleystein pegmatite Province, the granitic pegmatite and pegmatite are proved to be formed in specified geodynamic units and have distinct mineralization combinations with Sn-W restricted to the former and absent in the latter. The striking contrast between granitic pegmatite and pegmatite is ascribed to their discrepant geodynamic settings and the diminishing impact of the mantle towards the collision zone (Dill, 2015a).

5.4. Potential source of rare metals in metasedimentary rocks

Luan et al. (1995) proposed that multiple phases of metamorphic-tectonic-magmatic activities facilitate the mobilization and enrichment of Li, Be, Nb and Ta in sediments. Recently, Shen et al. (2015) investigated the rare-metal (Li, Be, Nb and Ta) potential of the Paleozoic sediments, including the Habahe Group, the Kulumuti Group, the Kemuqi Group, the Supute Group, the Aletai Formation, the Kangbutiebao Formation, the Kumasu Formation and the Hongshanzui Formation, for pegmatites in the Chinese Altai. The results show that all these sedimentary rocks have abundances of Li more than 1.6 times that of the average upper crust. They therefore proposed that the Li-rich sedimentary rocks could be the potential source of Li for the rare metal pegmatites in the Chinese Altai. Zhang et al. (2016) suggested that the rare-metal pegmatites from the Kaluan, Azubai and Jiamukai mining areas in the Central Altai domain originated from the partial melting of 38–83 wt% Halong granite and 17–62 wt% of the Kulumuti Group, according to calculated simulations based on their Hf isotopic compositions.

Recent works document that the metasedimentary rocks in the Chinese Altai consist of the Ordovician Habahe Group, Baihaba Formation and Doxilieke Formation, the Silurian Kulumuti Group, the Devonian Aletai and Kangbutiebao Formations, and the Carboniferous Hongshanzui and Kumasu Formations (Long et al., 2007, 2010, 2012; Jiang et al., 2010, 2011; Wang et al., 2014b). The Kemuqi and Fuyun Groups, which had been classified as Proterozoic strata (BGMRX, 1993), are demonstrated to have been deposited during the Ordovician to Silurian (Long et al., 2007, 2012). In the Chinese Altai, the rare metal pegmatite, especially the spodumene- and/or lepidolite-bearing pegmatites (such as the Li-rich pegmatites in Kaluan, Kelumute and Koktokay), are mainly distributed in the Central Altai domain, which is mostly occupied by the Habahe and Kulumuti Groups. In the Qiongkuer domain where a few of rare metal pegmatites (such as the Li-rich pegmatites in Xiaokalasu and Weizigou) are located, the Aletai Formation is widely exposed. It is therefore necessary to consider their source potential for rare-metal pegmatites.

The Habahe Group is the oldest and most extensive lithological unit in the Altai Orogenic Belt and extends for approximately 2500 km from the Chinese and Mongolian Altai in the southeast to the Russian and Kazakh Altai in the northwest. The early Paleozoic Barrovian-type metamorphic zonation that developed in the Habahe Group indicates that its maximum burial depth reached greater than 30 km (Wei and Wang, 2007; Jiang et al., 2015, 2016). In the Chinese Altai, it is widely exposed in the Central Altai domain and consists mainly of quartzo-feldspathic clastic turbidites (He et al., 1990; BGMRX, 1993; Windley et al., 2002; Li et al., 2006). In the Halong area, the group consists of schist, gneiss, migmatite and minor marble, overlain by the Kulumuti Group. In the Qinghe area, the group is composed of the lower garnet-sillimanite-biotite-plagioclase gneiss, garnet-biotite schist, migmatite, and leptynite and the upper staurolite-biotite schist, biotite-quartz schist, and chlorite-quartz schist. The deposition of the Habahe Group has recently been confirmed at 438 Ma for the western part and at 474 Ma for the eastern part of the Central Altai domain by detrital zircon U-Pb ages (Long et al., 2007, 2010). The Kulumuti Group is mainly exposed in the middle part of the Central Altai domain and consists of mica schist, quartz schist and quartzite for the Lower Group and metasandstone, metasiltstone and quartz sandstone for the Upper Group. Recent work suggests it was mainly deposited during the middle-late Ordovician and is equivalent to the eastern Habahe Group (Wang et al., 2014b). The Altai Formation is thought to have been deposited in a forearc basin (Windley et al., 2002) and consists of the lower clasolite, limestone, acidic volcanic rock, and tuff and the upper garnet-sillimanite gneiss, clasolite, calcareous sandstone and limestone. The zircon U-Pb ages of 365–354 Ma obtained from *meta*-rhyolite rocks indicate the Altai Formation was deposited in the late Devonian (Geng et al., 2010). Therefore, the Aletai Formation is too young to be the source of the *syn*-orogenic pegmatites in this work.

Detrital zircon ages and Hf isotopes suggest that the sediments in the Chinese Altai have multiple sources that consist of early Paleozoic arc-related igneous rocks and some ancient components from the adjacent Tuva-Mongolian block. Their terrigenous sedimentary components, varying detrital zircon ages and Hf isotopes suggest that they are chemically immature and compositionally similar to graywacke (Fig. 10) (Long et al., 2007, 2010, 2012; Jiang et al., 2011; Wang et al., 2014b). As noted above, the middle Paleozoic pegmatites and most granites from the Chinese Altai have a common source from immature crust (Fig. 8). Therefore, the early Paleozoic volcanic-sedimentary formations, especially the Habahe Group, can provide the major source for the granites and pegmatites, with or without injection of minor mantle components (Cai et al., 2011a; Liu et al., 2012; Jiang et al., 2016).

5.5. Tectonic setting and petrogenesis of pegmatite

As noted above, the Chinese Altai is a Paleozoic magmatic arc at an active margin and mainly consists of the Paleozoic volcanic-sedimentary formations and the Paleozoic-Mesozoic igneous rocks. It has undergone four orogenic stages, including the middle Cambrian-middle Silurian (500–430 Ma) preorogenic stage, late Silurian-Devonian (420–360 Ma) synorogenic stage, Carboniferous-Permian (350–250 Ma) lateorogenic stage and Triassic-early Jurassic (250–180 Ma) post-orogenic stage (Chen et al., 2006; Briggs et al., 2007; Xiao et al., 2006, 2008, 2009, 2010, 2015; Yuan et al., 2007; Cai et al., 2011a, b, 2012a, 2012b, 2016; Lv et al., 2012; Li et al., 2014; Zheng et al., 2012, 2015, 2017; Zhang et al., 2016). Correspondingly, the various types' pegmatitic rocks in the Chinese Altai can be identified by their origins and geodynamic settings (Table 1). The Devonian-early Carboniferous (403–330 Ma) rare metal pegmatites in this work have formed in a *syn*-orogenic subduction setting. Compare to the late- and postorogenic pegmatites, these synorogenic pegmatites have smaller scales and lower numbers and mineralization grades (Fig. 7). It is therefore stated that the post-orogenic setting is significant for the formation of the rare metal pegmatites in the Chinese Altai, which is consistent with the required tectonic setting for rare metal pegmatites worldwide (Černý, 1991b; Černý and Ercit, 2005; Tkachev, 2011; McCauly and Bradley, 2014; Zagorsky et al., 2014; Dill, 2015a, b; 2016; Bradley and McCauly, 2016).

According to current statistics on ages and locations of the rare metal pegmatites in the Chinese Altai, the middle Paleozoic synorogenic (403–330 Ma) and the Permian lateorogenic pegmatites are mainly concentrated in the Qiongkuer domain of the southern Chinese Altai. In contrast, the Triassic post-orogenic pegmatites are widely distributed in the Central Altai and the Qiongkuer domains, and the Jurassic pegmatites are found only in the Central Altai domain (Figs. 6 and 7). Zircon Hf isotope compositions show that the *syn*-orogenic pegmatites (403–330 Ma) have positive $\varepsilon_{Hf}(t)$ values of +2.06–+8.28 and old T_{DM2} ages of 1,234–860 Ma (this work). In comparison, the post-orogenic pegmatites (238–211 Ma) from the Central Altai show

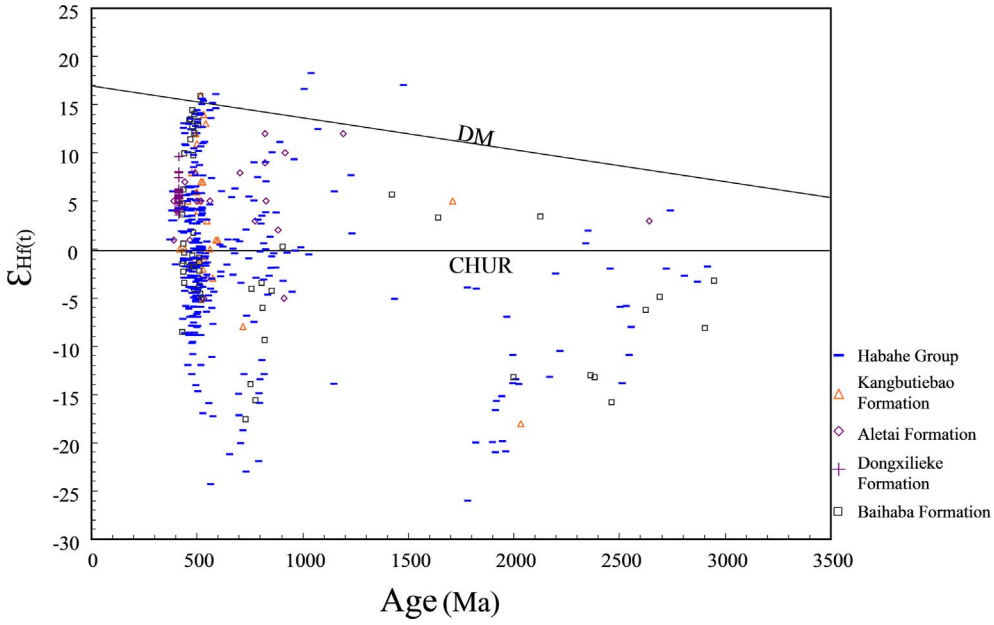

Fig. 10. Diagram of εHf(t) values versus crystallizing ages for zircons from the metasediments in the Chinese Altai. DM = depleted mantle, CHUR = chondrite uniform reservoir. Zircon data of the metasediments from Long et al., 2007, 2010, 2012; Jiang et al., 2011; Wang et al., 2014b.

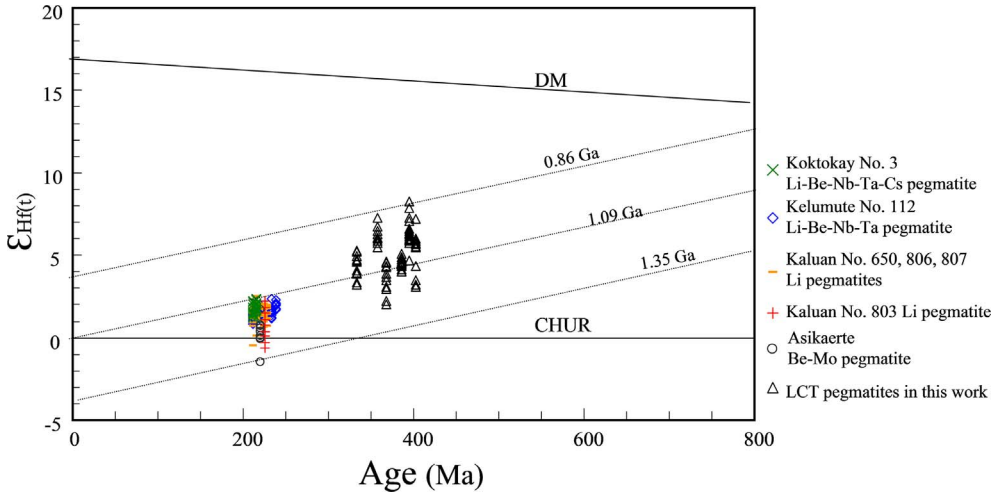

Fig. 11. Diagram of εHf(t) values versus crystallizing ages for zircons from the pegmatites in the Chinese Altai. DM = depleted mantle, CHUR = chondrite uniform reservoir. Data from Chen, 2011; Lv et al., 2012; Liu, 2015; Ma et al., 2015; Zhang et al., 2016 and this work.

lower $\varepsilon_{Hf}(t)$ values of −1.50–+2.50 and older T_{DM2} ages of 1,350–1090 Ma (Chen, 2011; Lv et al., 2012; Ma et al., 2015; Liu, 2015; Zhang et al., 2016) (Fig. 11). The Hf isotopic features and spatial-temporal distributions of the pegmatites indicate that (1) the syn- and post-orogenic pegmatites in the Chinese Altai have a common source mainly from immature crust represented by the early Paleozoic metasedimentary rocks, but the source of the *syn*-orogenic pegmatites contained more juvenile components; and (2) distinct tectonic-thermal dynamic mechanisms led to the specific spatial-temporal distributions of the syn- and post-orogenic pegmatites in the Chinese Altai.

In addition to the origin of pegmatite from granitic melt differentiation, anatexis has been regarded as an alternative mechanism (Norton, 1973; Breaks et al., 1978; Černý, 1991b) and has been increasingly confirmed in recent years (Martin and De Vito, 2005; Martin, 2007; Müller et al., 2016; Simmons, 2016; Simmons and Falster, 2016). Anatexis refers to partial melting of Li-enriched metasedimentary rocks that would presumably yield Li-rich magma at temperatures lower than those of haplogranite minima. The anatexis mechanism suggests that pegmatites are the products of low-percentage partial melting at low temperatures, whereas the associated granites are assumed to be products of high-percentage partial melting, presumably generated later in the same progressive anatectic event (Norton, 1973; Breaks et al., 1978). Martin and De Vito (2005) suggest that anatectic pegmatites may arise from crustal rocks and mantle rocks, and the distinction between anatectic pegmatites and fractionated pegmatites is the scale of the source magma. Dill (2015a) proposes that the rare metal pegmatite can't be simply derived from one single rock, but is the result of distinct multi-phase processes that bring elements together from various sources before anatexis.

According the geodynamic settings, pegmatites are classified as Alpine, Variscan, Rift, Andean and Island arc types (Dill, 2015a,b; 2016; 2018). No matter what type it is, the thickened crust induced by ensialic orogenic process is beneficial to producing pegmatite (Dill, 2016, 2018). Previous works documented that the Paleozoic Chinese Altai is similar to Japan-type island arc (Xiao et al., 2004, 2009, 2015). The orogenic process dominated by subduction-related accretions of magmatic arcs, island arcs, accretionary wedges, ophiolitic slices, and/or microcontinents from the middle Cambrian to Permian (Xiao et al.,

2008, 2015), and the massive granitoid production without massive continental-crust growth (Cai et al., 2011a; Liu et al., 2012; Jiang et al., 2016), indicating the ensialic orogenic character of the Chinese Altai. In addition, seismic data prove that the total crustal thickness of the Chinese Altai reach to ca.55 km (Wang et al., 2003a,b). Combining this work with the previous studies of granites, metasedimentary rocks and pegmatites noted above, we propose the following models for the petrogenesis of the *syn*-orogenic pegmatites in the Chinese Altai. During the oceanic ridge subduction in the Devonian (Windley et al., 2007; Sun et al., 2009; Cai et al., 2010, 2011a, b), the upwelling of asthenosphere via a slab window induced a significant injection of heat energy and mantle-derived materials into the Chinese Altai arc. The process gave rise to the generation of the Keketuohai and Habahe mafic rocks produced by partial melting of the lithospheric mantle (Cai et al., 2010, 2012), high-temperature metamorphism (Zheng et al., 2007; Jiang et al., 2010) and the formation of abundant granites induced by high-percentage partial melting of the early Paleozoic sediments (Windley et al., 2007; Yuan et al., 2007; Sun et al., 2008, 2009; Cai et al., 2011a, b; Yu et al., 2017). At the southern margin of the Chinese Altai, the Qiongkuer domain was in a forearc extensional setting represented by a series of fault-depression basins during the Devonian-early Carboniferous (Windley et al., 2002; Yuan et al., 2007; Yang et al., 2013). Low-percentage partial melting of metasedimentary rocks induced by decompression and limited injection of heat energy and mantle-derived materials caused the generation of thepegmatite-forming melts. They mobilized along faults, lithological boundaries and fault-related domal structures, intruded into the fissures of upper sedimentary rocks and the joints of early granites, and finally formed the *syn*-orogenic pegmatites (Fig. 12). High-percentage partial melting induced by high temperatures may have limited the generation of pegmatite-forming melts in the Central Altai, but low-percentage partial melting induced by decompression provided the possibility of pegmatite-forming melts in the Qiongkuer domain. Regarding the mechanism responsible for the effective concentration of rare-metal elements in pegmatite-forming melts without the gradual crystallization differentiation from parental granite melts, two more acceptable options appear to be (a) deep fluid-melt interaction during the melting process (Zagorsky, 2007, 2009) and (b) liquid immiscibility (Martin and De Vito, 2005; Martin, 2007; Zagorsky, 2007), which may occur during the dehydration melting process.

6. Conclusions

(1) According to the CMS (Chemical composition-Mineral assemblage-Structural geology) classification, the pegmatitic rocks in the Chinese Altai can be preliminarily divided into five types, including metapegmatite, pegmatoid, pegmatite, pseudopegmatite and granite pegmatite;

(2) Six rare metal pegmatites in the Chinese Altai, including JMHB02, QBL02, TLT01, ALJK01, AMLG01 and TMLT01, are identified by their CMS features, and dated by zircon U-Pb at 394.8 ± 4.0 Ma, 402.6 ± 5.5 Ma, 385.9 ± 3.5 Ma, 368.0 ± 4.0, 358.3 ± 4.6 Ma and 333.0 ± 6.0 Ma, respectively, indicating that they were formed in a *syn*-orogenic setting;

(3) Zircon Hf isotope compositions of the *syn*-orogenic pegmatites have positive $\varepsilon_{Hf(t)}$ values of + 2.06 - +8.28 and old T_{DM2} ages of

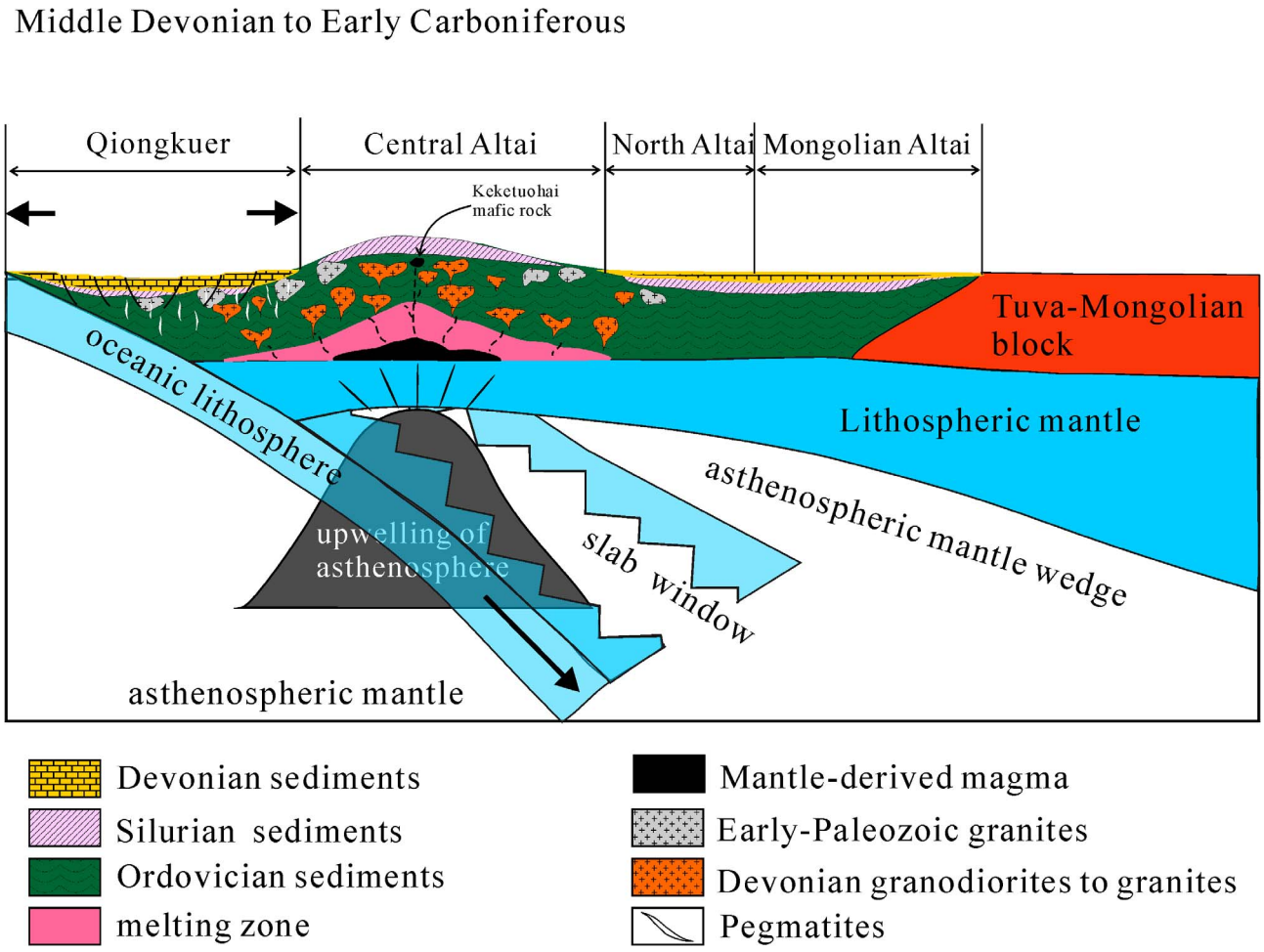

Fig. 12. The petrogenetic model for the *syn*-orogenic pegmatites in the Chinese Altai at Middle Devonian to Early Carboniferous. Modified from Sun et al., 2008 and Jiang et al., 2016.

1,234–860 Ma and are consistent with the Hf isotope compositions of most of the *syn*-orogenic I- and S-granites, which indicates that the pegmatites and granites are derived from a common immature crustal source from the early Paleozoic metasedimentary rocks by distinct tectonic-thermal dynamic mechanisms;

(4) Compared with the post-orogenic rare metal pegmatites in the Central Altai domain, the *syn*-orogenic pegmatites in this work show larger positive $\varepsilon_{Hf}(t)$ values and younger T_{DM2} ages, indicating more juvenile mantle components involved in their magma source. Combining this study with previous works, we suggest that the low-percentage partial melting of sediments induced by decompression and limited injection of heat energy and mantle-derived materials under a forearc extensional setting led to the formation of the *syn*-orogenic rare metal pegmatites in the Qiongkuer domain of the Chinese Altai.

Acknowledgments

We thank Profs. Xiaoming Liu and Honglin Yuan for their helps in the determinations of zircon U-Pb age and Hf isotopes. We also thank Editor-In-Chief Franco Pirajno, Assoc. Editor Harald G. Dill and Profs. Adam Pieczka and Miguel A. Galliski for their constructive comments. This study is jointly supported by the National Science Foundation of China under Grants 41372104 and 41403016.

Appendix A. Supplementary data

Supplementary data associated with this article can be found, in the online version, at http://dx.doi.org/10.1016/j.oregeorev.2018.02.022.

References

Andersen, T., 2002. Correction of common Pb in U-Pb analyses that do not report 204Pb. Chem. Geol. 192, 59–79.

Annikova, I.Y., V1adimirov, A.G., Vystavnoi, S.A., Zhuravlev, D.Z., Kruk, N.N., Lepekhina, E.N., Matukov, D.I., Moroz, E.N., Palesskii, S.V., Ponomarehuk, V.A., Rudnev, S.N., Sergeev, S.A., 2006. U-P b and A r/Ar dating and Sm-Nd and Pb-Pb isotopic study of the Kalguty molybdenum-tungsten ore-magmatic system, Southern Altai. Petrologiya 14(1), 90–108 (in Russian).

BGMRX (Bureau of Geology and Mineral Resources of Xinjiang Uygur Autonomous Region), 1993. Regional geology of Xinjiang Uygur Autonomous Region. People's Republic of China, Ministry of Geology and Mineral Resources. Geological Memoirs, Series, vol. 1, No. 32. Geological Publishing House, Beijing, pp. 6–206 (in Chinese).

Bradley, D.C., McCauley, A., 2016. Tectonic Settings of LCT Pegmatites in the Context of the Supercontinent Cycle. Second Eugene E. Foord Pegmatite Symposium 14–17.

Breaks, F.W., Bond, W.D., Stone, D., 1978. Preliminary geological synthesis of the English River subprovince: northwestern Ontario and its bearing upon mineral exploration. Ontario Geol. Surv. 72, 1–55.

Briggs, S.M., Yin, A., Manning, C.E., Chen, Z.L., Wang, X.F., Grove, M., 2007. Late Paleozoic tectonic history of the Ertix Fault in the Chinese Altai and its implications for the development of the Central Asian Orogenic System. Geol. Soc. Am. Bull. 119, 944–960.

Briggs, S.M., Yin, A., Manning, C.E., Chen, Z.L., Wang, X.F., 2009. Tectonic development of the southern Chinese Altai Range as determined by structural geology, thermobarometry, 40Ar/39Ar thermochronology, and Th/Pb ion-microprobe monazite geochronology. Geol. Soc. Am. Bull. 121, 1381–1393.

Cai, K., Sun, M., Jahn, B.M., Xiao, W., Long, X., Chen, H., Xia, X., Chen, M., Wang, X., 2016. Petrogenesis of the Permian Intermediate-Mafic Dikes in the Chinese Altai, Northwest China: Implication for a Postaccretion Extensional Scenario. J. Geol. 124, 481–500.

Cai, K., Sun, M., Yuan, C., Xiao, W., Zhao, G., Long, X., Wu, F., 2012. Carboniferous mantle-derived felsic intrusion in the Chinese Altai, NW China: implications for geodynamic change of the accretionary orogenic belt. Gondwana Res. 22, 681–698.

Cai, K., Sun, M., Yuan, C., Xiao, W., Zhao, G., Long, X., Wu, F., 2010. Geochronological and geochemical study of mafic dykes from the northwest Chinese Altai: implications for petrogenesis and tectonic evolution. Gondwana Res. 18, 638–652.

Cai, K.D., Sun, M., Yuan, C., Zhao, G.C., Xiao, W.J., Long, X.P., 2012b. Keketuohai mafic-ultramafic complex in the Chinese Altai, NW China: petrogenesis and geodynamic significance.

Cai, K.D., Sun, M., Yuan, C., Zhao, G.C., Xiao, W.J., Long, X.P., Wu, F.Y., 2011a. Geochronology, petrogenesis and tectonic significance of peraluminous granites from the Chinese Altai, NW China. Lithos 127, 261–281.

Cai, K.D., Sun, M., Yuan, C., Zhao, G.C., Xiao, W.J., Long, X.P., Wu, F.Y., 2011b. Prolonged magmatism, juvenile nature and tectonic evolution of the Chinese Altai, NW China: evidence from zircon U-Pb and Hf isotopic study of Paleozoic granitoids. J. Asian Earth Sci. 42, 949–968.

Černý, P., 1991a. Rare-element granite pegmatites. Part I: anatomy and internal evolution of pegmatite deposits. Geosci. Canada 18, 49–67.

Černý, P., 1991b. Rare-element granitic pegmatites. Part II: regional to global environments and petrogenesis. Geosci. Canada 18, 68–81.

Černý, P., London, D., Novák, M., 2012. Granitic pegmatites as reflections of their sources. Elements 8, 289–294.

Černý, P., Ercit, T.S., 2005. The classification of granitic pegmatites revisited. Canadian Mineral. 43, 2005–2026.

Černý, P., Halden, N.M., Ferreira, K., Meintzer, R.E., Brisbin, W.C., Chackowsky, L.E., Corkery, M.T., Longstaffe, F.J., Trueman, D.L., 2012. Extreme fractionation and deformation of the leucogranite-pegmatite suite at Red Cross lake, Manitoba, Canada. II. Petrology of the leucogranites and pegmatites. Canadian Mineral. 50, 1807–1822.

Cuney, M., Alexandrov, P., de Veslud, C.L.C., Cheilletz, A., Raimbault, L., Ruffet, G., Scaillet, S., 2002. The timing of W-Sn-rare metals mineral deposit formation in the Western Variscan chain in their orogenic setting: the case of the Limousin area (Massif Central, France). Geolog. Soc. Lond. Spec. Publ. 204 (1), 213–228.

Chai, F.M., Dong, L.H., Yang, F.Q., Liu, F., Geng, X.X., 2010. Age, geochemistry and petrogenesis of tiemierte granites in the Kelang basin at eht southern margin of Altay, Xinjiang. Acta Petrologica Sinica 26 (2), 377–386.

Che, X.D., Wu, F.Y., Wang, R.C., Gerdes, A., Ji, W.Q., Zhao, Z.H., Yang, J.H., Zhu, Z.Y., 2015. In situ U-Pb isotopic dating of columbite–tantalite by LA–ICP–MS. Ore Geol. Rev. 65, 979–989.

Chen, B., Jahn, B.M., 2002. Geochemical and isotopic studies of the sedimentary and granitic rocks of the Altai orogen of NW China and their tectonic implications. Geol. Mag. 139, 1–13.

Chen, F.W., Li, H.Q., Wang, D.H., Cai, H., Chen, W., 1999. New chronological evidence for Yanshanian diagenetic mineralization in China's Altay orogenic belt. Chin. Sci. Bull. 44, 1142–1148.

Chen, H.L., Li, Z.L., Yang, S.F., Dong, C.W., Xiao, W.J., Tainosho, Y., 2006. Mineralogical and geochemical study of a newly discovered mafic granulite, northwest China: Implications for tectonic evolution of the Altay Orogenic Belt. Island Arc 15, 210–222.

Chen, J.F., 2011. Geochemistry of the plate part in Altai No. 3 pegmatite and its formation and evolution. A dissertation submitted to Graduate University of Chinese Academy of Sciences for the degree of Master of Philosophy, pp. 1–86 (in Chinese with English abstract).

Dill, H., 2015a. The Hagendorf-Pleystein Province: the center of pegmatites in an ensialic orogen. Springer 15, 1–465.

Dill, H.G., 2015b. Pegmatites and aplites: Their genetic and applied ore geology. Ore Geol. Rev. 69, 417–561.

Dill, H.G., 2016. The CMS classification scheme (Chemical composition-Mineral assemblage-Structural geology)-linking geology to mineralogy of pegmatitic and aplitic rocks. Neues Jahrbuch für Mineralogie-Abhandlungen: J. Mineral. Geochem. 193 (3), 231–263.

Dill, H.G., 2018. Geology and chemistry of Variscan-type pegmatite systems (SE Germany)-With special reference to structural and chemical pattern recognition of felsic mobile components in the crust. Ore Geol. Rev. 92, 205–239.

Diwu, C., Sun, Y., Guo, A., Wang, H., Liu, X., 2011. Crustal growth in the North China Craton at ~ 2.5 Ga: Evidence from in situ zircon U-Pb ages, Hf isotopes and whole-rock geochemistry of the Dengfeng complex. Gondwana Res. 20, 149–170.

Geng, X.X., Chai, F.M., Yang, F.Q., Zuo, W.Z., Guo, Z.L., Liu, F., Zhang, Z.X., 2010. Geochronology and genesis of the bimodal volcanic rocks in Dalawuzi from the southern margin of Altay, Xinjiang. Acta Petrologica Sinica 26, 2967–2980 (in Chinese with English abstract).

Griffin, W.L., Pearson, N.J., Belousova, E.A., Saeed, A., 2006. Comment: Hf-isotope heterogeneity in zircon 91500. Chem. Geol. 233, 358–363.

Han, B.F., 2008. A preliminary comparison of Mesozoic granitoids and rare metal deposits in Chinese and Russian Altai Mountains. Acta Petrologica Sinica 24 (4), 655–660 (in Chinese with English abstract).

Han, B.F., Wang, S.G., Jahn, B.M., Hong, D.W., Kagami, H., Sun, Y.L., 1997. Depleted-mantle source for the Ulungur River A-type granites from North Xinjiang, China: geochemistry and Nd-Sr isotopic evidence, and implications for Phanerozoic crustal growth. Chem. Geol. 138, 135–159.

Han, C., Xiao, W., Zhao, G., Su, B., Sakyi, P.A., Ao, S.J., Wan, B., Zhang, J.E., Zhang, Z.Y., Wang, Z.M., 2014. Mid-Late Paleozoic metallogenesis and evolution of the Chinese Altai and East Junggar Orogenic Belt, NW China, Central Asia. J. Geosci. 59, 255–274.

He, G.Q., Han, B.F., Yue, Y.J., Wang, J.H., 1990. Tectonic division and crustal evolution of Altay orogenic belt in China. Geosci. Xinjiang 2, 9–20 (in Chinese with English abstract).

Hu, A.Q., 2006. SHRIMP zircon U-Pb dating and its significance for gneisses from the southeast area to Qinghe Country in the Altai, China. Acta Petrologica Sinica 22, 1–10 (in Chinese with English abstract).

Hu, A.Q., Jahn, B.M., Zhang, G.X., Chen, Y.B., Zhang, Q.F., 2000. Crustal evolution and Phanerozoic crustal growth in northern Xinjiang: Nd isotopic evidence. Part I: isotopic characterization of basement rocks. Tectonophysics 328, 15–51.

Jahn, B.M., Wu, F., Chen, B., 2000. Granitoids of the Central Asian Orogenic Belt and continental growth in the Phanerozoic. Geol. Soc. Am. Spec. Pap. 350, 181–193.

Jahns, R.H., Burnham, C.W., 1969. Experimental studies of pegmatite genesis I: a model for the derivation and crystallization of granitic pegmatites. Econ. Geol. 64, 843–864.

Jiang, L.P., 2012. The study on fluid inclusion of Liangkeshu pegmatite iron deposit in Altay. Urumchi: A Dissertation Submitted to Xinjiang University for the Degree of Master of. Philosophy 1–50 (in Chinese with English abstract).

Jiang, Y., Štípská, P., Sun, M., Schulmann, K., Zhang, J., Wu, Q., Long, X., Yuan, C., Racek, M., Zhao, G., Xiao, W., 2015. Juxtaposition of Barrovian and migmatite domains in the Chinese Altai: a result of crustal thickening followed by doming of partially molten lower crust. J. Metamorphic Geol. 33, 45–70.

Jiang, Y., Sun, M., Zhao, G., Yuan, C., Xiao, W., Xia, X., Long, X., Wu, F., 2010. The ~390 Ma high-T metamorphic event in the Chinese Altai: A consequence of ridge-subduction? Am. J. Sci. 310, 1421–1452.
Jiang, Y., Sun, M., Zhao, G., Yuan, C., Xiao, W., Xia, X., Long, X., Wu, F., 2011. Precambrian detrital zircons in the Early Paleozoic Chinese Altai: their provenance and implications for the crustal growth of central Asia. Precambr. Res. 189, 140–154.
Jiang, Y., Schulmann, K., Sun, M., Štípská, P., Guy, A., Janoušek, V., Lexa, O., Yuan, C., 2016. Anatexis of accretionary wedge, Pacific-type magmatism, and formation of vertically stratified continental crust in the Altai Orogenic Belt. Tectonics 35 (12), 3095–3118.
Li, C., Zhang, M., Fu, P., Qian, Z., Hu, P., Ripley, E., 2012. The Kalatongke magmatic Ni-Cu deposits in the Central Asian Orogenic Belt, NW China: product of slab window magmatism? Mineralium Deposita 47, 51–67.
Li, H.J., He, G.Q., Wu, T.R., Wu, B., 2006. Confirmation of Altai-Mongolia microcontinent and its implications. Acta Petrologica Sinica 22, 1369–1379 (in Chinese with English abstract).
Li, X.R., Liu, F., Yang, F.Q., 2012. Geologyical times and tis signification of th two mica syenogranite in the Keyinblak Cu-Zn deposit area in Altay, Xinjiang. Xinjiang Geol. 30 (1), 5–11.
Li, Z., Li, Y., Chen, H., Santosh, M., Xiao, W., Wang, H., 2010. SHRIMP U-Pb zircon chronology of ultrahigh-temperature spinel-orthopyroxene-garnet granulite from South Altay orogenic belt, northwestern China. Island Arc 19, 506–516.
Li, Z., Yang, X., Li, Y., Santosh, M., Chen, H., Xiao, W., 2014. Late Paleozoic tectono-metamorphic evolution of the Altai segment of the Central Asian Orogenic Belt: Constraints from metamorphic P-T pseudosection and zircon U–Pb dating of ultra-high-temperature granulite. Lithos 204, 83–96.
Liu, F., Yang, F.Q., Mao, J.W., Chai, F.M., Geng, X.X., 2009. Study on chronology and geochemistry for Abagong granite in Altay orogen. Acta Petrologica Sinica 25, 1416–1425 (in Chinese with English abstract).
Liu, F., Zhang, Z.X., Li, Q., Zhang, C., Li, C., 2014. New precise timing constraint for the Keketuohai No. 3 pegmatite in Xinjiang, China, and identification of its parental pluton. Ore Geol. Rev. 56, 209–219.
Liu, G.R., Dong, L.H., Gao, F.P., Chen, J.X., Zhao, H., Wang, D.S., Song, Z.Y., Qin, J.H., 2010. LA-ICP-MS U-Pb zircon dating and geochemistry of the Devonian granites from the middle Kelan river valley of the Altay in Xinjiang. Acta Geoscientica Sinica 31 (4), 519–531.
Liu, H., 2013. Geochemical study on petrogenesis of Aral granite and the Keketuohai No. 3 pegmatite vein, Altay, Xinjiang. A dissertation submitted to the Kunming University of Science and Technology for the degree of Master of Philosophy, pp. 1–60 (in Chinese with English abstract).
Liu, W., Liu, X.J., Xiao, W.J., 2012. Massive granitoid production without massive continental-crust growth in the Chinese Altay: Insight into the source rock of granitoids using integrated zircon U-Pb age, Hf–Nd–Sr isotopes and geochemistry. Am. J. Sci. 312 (6), 629–684.
Liu, W.Z., 2015. The geochemical evolution of the Asikaerte granite-pegmatite system and its implication for the metallogenesis of Be and Mo, XinJiang, China. Guiyang: A Dissertation Submitted to Institute of Geochemistry for the Degree of Master of. Philosophy 1–71 (in Chinese with English abstract).
Liu, Y.L., Zhang, H., Tang, Y., Zhang, X., Lv, Z.H., Zhao, J.Y., 2017. Petrogenesis and tectonic setting of the Middle Permian A-type granites in Altay, Northwestern China: evidences from geochronological, geochemical, and Hf isotopic studies. Geol. J in press.
Liu, Y.S., Gao, S., Hu, Z.C., Gao, C.G., Zong, K.Q., Wang, D.B., 2009. Continental and oceanic crust recycling-induced melt-peridotite interactions in the Trans-North China Orogen: U-Pb dating, Hf isotopes and trace elements in zircons from mantle xenoliths. J. Petrol. 51, 537–571.
London, D., 2005. Granitic pegmatites: an assessment of current concepts and directions for the future. Lithos 80, 281–303.
London, D., 2008. Pegmatites. Can. Mineral. Special Publication 10, 1–347.
London, D., 2014. A petrologic assessment of internal zonation in granitic pegmatites. Lithos 184–187, 74–104.
Long, X.P., Sun, M., Yuan, C., Xiao, W.J., Lin, S.F., Wu, F.Y., Xia, X.P., Cai, K.D., 2007. U-Pb and Hf isotopic study of zircons from metasedimentary rocks in the Chinese Altai: implications for Early Paleozoic tectonic evolution. Tectonics, TC5015, DOI: 10.1029/2007TC002128.
Long, X.P., Sun, M., Yuan, C., Xiao, W.J., Cai, K.D., 2008. Early Paleozoic sedimentary record of the Chinese Altai: Implications for its tectonic evolution. Sediment. Geol. 208, 88–100.
Long, X.P., Yuan, C., Sun, M., Xiao, W.J., Zhao, G.C., Wang, Y.J., Cai, K.D., 2010. Detrital zircon ages and Hf isotopes of the early Paleozoic Flysch sequence in the Chinese Altai, NW China: New constraints on depositional age, provenance and tectonic evolution. Tectonophysics 480, 213–231.
Long, X., Yuan, C., Sun, M., Safonova, I., Xiao, W., Wang, Y., 2012. Geochemistry and U-Pb detrital zircon dating of Paleozoic graywackes in East Junggar, NW China: insights into subduction–accretion processes in the southern Central Asian Orogenic Belt. Gondwana Res. 21, 637–653.
Luan, S.W., Mao, Y.Y., Fan, L.M., Wu, X.B., Lin, J.H., 1995. Rare metal mineralization and exploration in the Keketuohai Area. Chengdu Press Chengdu Univ. Sci. Technol. 1–278 (in Chinese with English abstract).
Ludwig, K.R., 2003. User's manual for Isoplot/Ex, Version 3. 00. A Geochronological Toolkit for Microsoft Excel: Berkeley Geochronology Center Special Publication 4, 1–70.
Lv, Z.H., Zhang, H., Tang, Y., Guan, S.J., 2012. Petrogenesis and magmatic-hydrothermal evolution time limitation of Kelumute No. 112 pegmatite in Altay, Northwestern China: evidence from zircon U-Pb and Hf isotopes. Lithos 154, 374–391.
Lv, Z.H., Zhang, H., Tang, Y., 2015. The study of genesis relationship between Bieyesamasi No. L1 pegmatite Li-Nb-Ta ore deposit and wall rock granite, Xinjiang. Acta Mineralogica Sinica S1, p. 323 (in Chinese).
Lv, Z.H., Zhang, H., Tang, Y., Zhao, J.Y., Liu, Y.L., Guo, L., 2018. The Distribution of Phosphorous in Various Types of Pegmatites From Altai. Bulletin of Mineralogy, Petrology and Geochemistry. In press, Xinjiang and its implication (in Chinese with English abstract).
Ma, Z.L., Zhang, H., Tang, Y., Lv, Z.H., Zhang, X., Zhao, J.Y., 2015. Zircon U-Pb geochronology and Hf isotopes of pegmatites from the Kaluan mining area in the Altay, Xinjiang and their genetic relationship with the Halong granite. Geochimica 44, 9–26 (in Chinese with English abstract).
Marignac, C., Cuney, M., 1999. Ore deposits of the French Massif Central: insight into the metallogenesis of the Variscan collision belt. Mineralium Deposita 34 (5–6), 472–504.
Martin, R.F., 2007. The Importance of Tectonic Setting in Understanding Granitic Pegmatites. In Granitic Pegmatites: The State of the Art-International Symposium.
Martin, R.F., De Vito, C., 2005. The patterns of enrichment in felsic pegmatites ultimately depend on tectonic setting. Canadian Mineral. 43, 2027–2048.
McCauley, A., Bradley, D.C., 2014. The global age distribution of granitic pegmatites. Canadian Mineral. 183–190.
Müller, A., Romer, R.L., Szuszkiewicz, A., Ilnicki, S., Szełęg, E., 2016. Can pluton-related and pluton-unrelated granitic pegmatites be distinguished by their chemistry? Second Eugene E. Foord Pegmatite Symposium 67–69.
Niu, H.C., Xu, J.F., Yu, X.Y., Chen, F.R., Zheng, Z.P., 1999. Discovery of the Mg-rich volcanics in Altai, Xinjiang, and its geological implications. Chinese Sci. Bull. 44, 1002–1004.
Niu, H.C., Sato, H., Zhang, H.X., Ito, J., Yu, X.Y., Nagao, T., Terada, K., Zhang, Q., 2006. Juxtaposition of adakite, boninite, high-TiO_2 and low-TiO_2 basalts in the Devonian southern Altay, Xinjiang, NW China. J. Asian Earth Sci. 28, 439–456.
Norton, J.J., 1973. Lithium, cesium, and rubidium-the rare alkali metals. United States mineral resources: US Geological Survey Professional Paper 820, 365–378.
Pirajno, F., Mao, J., Zhang, Z., Zhang, Z., Chai, F., 2008. The association of mafic–ultramafic intrusions and A-type magmatism in the Tian Shan and Altay orogens, NW China: implications for geodynamic evolution and potential for the discovery of new ore deposits. J. Asian Earth Sci. 32, 165–183.
Qin, K.Z., Guo, Z.L., Shen, M.D., Tang, D.M., Zhou, Q.F., Wang, C.L., Guo, X.J., Tian, Y., Ding, J.G., 2013. Types, intrusive and mineralization ages of pegmatite rare-element deposits in Chinese Altay. Xinjiang Geol. 31, 1–7 (in Chinese with English abstract).
Qin, J.H., Geng, X.X., Wen, C.Q., Guo, J.X., Ren, Y.C., 2016. Zircon LA-ICP-MS U-Pb age of intrusion from Xiaotuergen copper deposit in Altay, Xinjiang, and its geological significance. Miner. Deposits 35, 18–32.
Ren, B.Q., Zhang, H., Tang, Y., Lv, Z.H., 2011. LA-ICPMS U-Pb zircon geochronology of the Altai pegmatites and its geological significance. Acta Mineralogica Sinica 31, 587–596 (in Chinese with English abstract).
Selway, J.B., Breaks, F.W., Tindle, A.G., 2005. A review of rare-element (Li-Cs-Ta) pegmatite exploration techniques for the Superior Province, Canada, and large world-wide tantalum deposits. Explor. Mining Geol. 14, 1–30.
Sengor, A.M.C., Natal'in, B.A., Burtman, V.S., 1993. Evolution of the Altaid tectonic collage and Palaeozoic crustal growth in Eurasia. Nature 364, 299–306.
Shen, R.F., Zhang, H., Tang, Y., Lv, Z.H., 2015. Geochemical characteristics of Paleozoic strata and its restriction on depositional environment in Altay orogen, north Xinjiang, China. Geochimica 44, 43–60 (in Chinese with English abstract).
Shen, X., Zhang, H., Wang, Q., Wyman, D.A., Yang, Y., 2011. Late Devonian-Early Permian A-type granites in the southern Altay Range, Northwest China: petrogenesis and implications for tectonic setting of "A2-type" granites. J. Asian Earth Sci. 42, 986–1007.
Simmons, W.B., 2016. REE-Rich Pegmatites from the South Platte and Trout Creek Pass Pegmatite Districts, Colorado: Contrasting Geochemical Profiles and Tectonic Regimes. In: Second Eugene E. Foord Pegmatite Symposium, pp. 95–102.
Simmons, W.B., Falster, A.U., 2016. Evidence for an Anatectic Origin of an LCT Type Pegmatite: Mt. In Second Eugene E. Foord Pegmatite Symposium, Mica, Maine, pp. 103.
Song, G.X., Qin, K.Z., Liu, T., Li, G., Shen, P., 2010. The U-Pb ages, Hf isotope and REE patterns of older zircon fron devonian volcanic rocks in Ashele basin of the southern margin of Altai orogen and its geological significance. Acta Petrologica Sinica 26 (10), 2946–2958.
Sun, M., Long, X., Cai, K., Jiang, Y., Wang, B., Yuan, C., Zhao, G.C., Xiao, W., Wu, F., 2009. Early Paleozoic ridge subduction in the Chinese Altai: insight from the abrupt change in zircon Hf isotopic compositions. Sci. China Ser. D: Earth Sci. 52, 1345–1358.
Sun, M., Yuan, C., Xiao, W.J., Long, X.P., Xia, X.P., Zhao, G.C., Lin, S.F., Wu, F.Y., Kroner, A., 2008. Zircon U-Pb and Hf isotopic study of gneissic rocks from the Chinese Altai: Progressive accretionary history in the early to middle Palaeozoic. Chem. Geol. 247, 352–383.
Tkachev, A.V., 2011. Evolution of metallogeny of granitic pegmatites associated with orogens throughout geological time. Geol. Soc. Lond. Spec. Publ. 350, 7–23.
Tong, Y., 2006. Geochronology, origin of the Late Paleozoic granitoids from the Altai Orogen in China and their geological significance. Beijing: A Dissertation Submitted to Chinese Academy of Geological Sciences for the Degree of Doctor of. Philosophy 1–112 (in Chinese with English abstract).
Tong, Y., Wang, T., Kovach, Hong, D.W., Han, B.F., 2006a. Age and origin of the Takeshiken postorogenic alkali-rich intrusive rocks in southern Altai, near the Mongolian border in China and its implications for continental growth. Acta Petrologica Sinica 22, 1267–1278 (in Chinese with English abstract).
Tong, Y., Hong, D.W., Wang, T., Wang, S.G., Han, B.F., 2006b. TIMS U-Pb zircon ages of Fuyun post-orogenic linear granite plutons on the southern margin of Altay orogenic belt and their implications. Acta Petrologica et Mineralogica 25, 85–89 (in Chinese

with English abstract).
Tong, Y., Wang, T., Hong, D.W., Dai, Y.J., 2007. Ages and origin of early Devonian granites from the north part of Chinese Altai Mountains and its tectonic implications. Acta Petrologica Sinica 23, 1933–1944 (in Chinese with English abstract).
Tong, Y., Wang, T., Siebel, W., Hong, D.W., Sun, M., 2012. Recognition of early Carboniferous alkaline granite in the southern Altai orogen: post-orogenic processes constrained by U-Pb zircon ages, Nd isotopes, and geochemical data. Int. J. Earth Sci. 101, 937–950.
Tong, Y., Wang, T., Jahn, B.M., Sun, M., Hong, D.W., Gao, J.F., 2014. Post-accretionary Permian granitoids in the Chinese Altai orogen: geochronology, petrogenesis and tectonic implications. Am. J. Sci. 314, 80–109.
Partington, G.A., McNaughton, N.J., Williams, I.S., 1995. A review of the geology, mineralization, and geochronology of the Greenbushes pegmatite, Western Australia. Econ. Geol. 90 (3), 616–635.
Vladimirov, A.G., Vystanvnoi, S.A., Tikov, A.V., Rudnev, S.N., Dergachev, V.B., Annikov, I.Y., Tikunov, Y.V., 1998. Petrology of the early Mesozoic rare-metal granites of the southern Gorny Altai. Geologiya i Geofizica 39 (7), 901–916 (in Russian with English abstract).
Wan, B., Xiao, W., Zhang, L., Windley, B.F., Han, C., Quinn, C.D., 2011. Contrasting styles of mineralization in the Chinese Altai and East Junggar, NW China: implications for the accretionary history of the southern Altaids. J. Geol. Soc. 168, 1311–1321.
Wang, D.H., Chen, Y.C., Xu, Z.G., 2001. Chronological study of Caledonian metamorphic pegmatite muscovite deposits in the Altay Mountains, northwestern China, and its significance. Acta Geological Sinica 75, 419–425 (in Chinese with English abstract).
Wang, D.H., Chen, Y.C., Xu, Z.G., 2002. Metallogenetic Series and Regularity of the Altay Metallogenic Province. Atomic Energy Press, Beijing, pp. 1–493 (in Chinese).
Wang, D.H., Chen, Y.C., Xu, Z.G., 2003. 40Ar/39Ar Isotope dating on Muscovites from Indosinian Rare-metal Deposits in Central Altay, Northwestern China. Bull. Mineral. Petrol. Geochem. 22, 14–17 (in Chinese with English abstract).
Wang, D.H., Chen, Y.C., Zou, T.R., Xu, Z.G., Li, H.Q., Chen, W., Chen, F.W., Tian, F., 2000. 40Ar/39Ar dating for the Azubai rare metal-gem deposit in Altay, Xinjiang: New evidence for Yanshanian mineralization of rare metals. Geol. Rev. 46, 307–311 (in Chinese with English abstract).
Wang, D.H., Zou, T.R., Xu, Z.G., Yu, J.J., 2004. Advance in the study of using pegmatite deposits as the tracer of orogenic process. Adv. Earth Sci. 19, 614–620 (in Chinese with English abstract).
Wang, T., Hong, D.W., Jahn, B.M., Tong, Y., 2006. Timing, petrogenesis, and setting of Paleozoic synorogenic intrusions from the Altai Mountains, Northwest China: Implications for the tectonic evolution of an accretionary orogen. J. Geol. 114, 735–751.
Wang, T., Tong, Y., Jahn, B.M., Zou, T.R., Wang, Y.B., Hong, D.W., Han, B.F., 2007. SHRIMP U-Pb Zircon geochronology of the Altai No. 3 Pegmatite, NW China, and its implications for the origin and tectonic setting of the pegmatite. Ore Geol. Rev. 32, 325–336.
Wang, T., Hong, D.W., Tong, Y., Han, B.F., Shi, Y.R., 2005. Zircon U-Pb SHRIMP age and origin of post-orogenic Lamazhao granitic pluton from Altai orogen: Its implications for vertical continental growth. Acta Petrologica Sinica 21, 640–650 (in Chinese with English abstract).
Wang, T., Jahn, B.M., Kovach, V.P., Tong, Y., Hong, D.W., Han, B.F., 2009. Nd-Sr isotopic mapping of the Chinese Altai and implications for continental growth in the Central Asian Orogenic Belt. Lithos 110, 359–372.
Wang, T., Tong, Y., Li, S., Zhang, J.J., Shi, X.J., Li, J.Y., Han, B.F., 2010. Spatial and temporal variations of granitoids in the Altay orogen and their implications for tectonic setting and crustal growth: perspectives from Chinese Altay. Acta Petrologica et Mineralogica 29, 595–618 (in Chinese with English abstract).
Wang, T., Jahn, B.M., Kovach, V.P., Tong, Y., Wilde, S.A., Hong, D.W., Li, S., Salnikova, E.B., 2014a. Mesozoic intraplate granitic magmatism in the Altai accretionary orogen, NW China: implications for the orogenic architecture and crustal growth. Am. J. Sci. 314, 1–42.
Wang, Y., Long, X., Wilde, S.A., Xu, H., Sun, M., Xiao, W., Yuan, C., Cai, K., 2014b. Provenance of Early Paleozoic metasediments in the central Chinese Altai: Implications for tectonic affinity of the Altai-Mongolia terrane in the Central Asian Orogenic Belt. Lithos 210, 57–68.
Wang, Y., Yuan, C., Long, X., Sun, M., Xiao, W., Zhao, G., Cai, K., Jiang, Y., 2011. Geochemistry, zircon U-Pb ages and Hf isotopes of the Paleozoic volcanic rocks in the northwestern Chinese Altai: petrogenesis and tectonic implications. J. Asian Earth Sci. 42 (5), 969–985.
Wang, Y.X., Mooney, W.D., Yuan, X.C., Coleman, R.G., 2003. The crustal structure from the Altai Mountains to the Altyn Tagh fault, northwest China. J. Geophys. Res. 108, 2322. http://dx.doi.org/10.1029/2001JB000552.
Wei, C., Wang, W., 2007. Phase equilibria in the process of anatexis in high-grade metapelites. Earth Sci. Front. 14, 1225–1234.
Wiedenbeck, M., Hanchar, J.M., Peck, W.H., Sylvester, P., Valley, J., Whitehouse, M., Kronz, A., Morishita, Y., Nasdala, L., Fiebig, J., Franchi, I., Giard, J.P., Greenwood, R.C., Hinton, R., Kita, N., Mason, P.R.D., Norman, M., Ogasawara, M., Piccoli, P.M., Rhede, D., Satoh, H., Schulz-Dobrick, B., Skar, O., Spicuzza, M.J., Terada, K., Tindle, A., Togashi, S., Vennemann, T., Xie, Q., Zheng, Y.F., 2004. Further characterisation of the 91500 zircon crystal. Geostandards Geoanal. Res. 28, 9–39.
Windley, B.F., Kroener, A., Guo, J., Qu, G., Li, Y., Zhang, C., 2002. Neoproterozoic to Paleozoic geology of the Altai Orogen, NW China: new zircon age data and tectonic evolution. J. Geol. 110, 719–737.
Windley, B.F., Alexeiev, D., Xiao, W.J., Kröner, A., Badarch, G., 2007. Tectonic models for accretion of the Central Asian Orogenic Belt. J. Geol. Soc. 164, 31–47.
Wu, B.Q., Zou, T.R., 1989. The genesis of granitic pegmatites in Xinjiang Altai. Miner. Geol. Xinjiang 1, 60–70 (in Chinese).
Wong, K., Sun, M., Zhao, G., Yuan, C., Xiao, W., 2010. Geochemical and geochronological studies of the Alegedayi Ophiolitic Complex and its implication for the evolution of the Chinese Altai. Gondwana Res. 18 (2–3), 438–454.
Xiao, W.J., Han, C.M., Yuan, C., Chen, H.L., Sun, M., Lin, S.F., Li, Z.L., Mao, Q.G., Zhang, J.E., Sun, S., Li, J.L., 2006. Unique Carboniferous-Permian tectonic-metallogenic framework of Northern Xinjiang (NW China): Constraints for the tectonics of the southern Paleoasian Domain. Acta Petrologica Sinica 22, 1062–1076 (in Chinese with English abstract).
Xiao, W.J., Han, C.M., Yuan, C., Sun, M., Lin, S.F., Chen, H.L., Li, Z.L., Li, J.L., Sun, S., 2008. Middle Cambrian to Permian subduction-related accretionary orogenesis of Northern Xinjiang, NW China: Implications for the tectonic evolution of central Asia. J. Asian Earth Sci. 32, 102–117.
Xiao, W.J., Huang, B.C., Han, C.M., Sun, S., Li, J.L., 2010. A key to understanding the architecture of accretionary orogens. Gondwana Res. 18, 253–273.
Xiao, W.J., Windley, B.F., Badarch, G., Sun, S., Qin, K.Z., 2004. Paleozoic accretionary and convergent tectonics of the southern Altaids: implications for the growth of Central Asia. J. Geol. Soc. 161, 339–342.
Xiao, W.J., Windley, B.F., Hao, J., Zhai, M.G., 2003. Accretion leadingto collision and the Permian Solonker suture, Inner Mongolia, China: Termination of the central Asian orogenic belt. Tectonics 22 (6), 1069. http://dx.doi.org/10.1029/2002TC00148.
Xiao, W.J., Windley, B.F., Huang, B.C., Han, C.M., Yuan, C., Chen, H.L., Sun, M., Sun, S., Li, J.Y., 2009. End-Permian to mid-Triassic termination of the accretionary processes of the southern Altaids: implications for the geodynamic evolution, Phanerozoic continental growth, and metallogeny of Central Asia. Int. J. Earth Sci. 98, 1189–1217.
Xiao, W., Windley, B.F., Sun, S., Li, J., Huang, B., Han, C., Yuan, C., Sun, M., Chen, H., 2015. A tale of amalgamation of three Permo-Triassic collage systems in Central Asia: Oroclines, sutures, and terminal accretion. Annu. Rev. Earth Planetary Sci. 43, 477–507.
Xu, J.G., Zou, T.R., 1975. A discussion on petrogenesis of granite pegmatites in Xinjiang Altai. Xinjiang Geol. 1, 60–70 (In Chinese).
Yang, F., Liu, F., Li, Q., Geng, X., 2014. In situ LA–MC–ICP–MS U-Pb geochronology of igneous rocks in the Ashele Basin, Altay orogenic belt, northwest China: Constraints on the timing of polymetallic copper mineralization. J. Asian Earth Sci. 79, Part A, 477–496.
Yang, F., Mao, J., Liu, F., Chai, F., Guo, Z., Zhou, G., Geng, X., Gao, J., 2010. Geochronology and geochemistry of the granites from the Mengku iron deposit, Altay Mountains, northwest China: implications for its tectonic setting and metallogenesis. Australian J. Earth Sci. 57, 803–818.
Yang, F., Mao, J., Liu, F., Chai, F., Geng, X., Zhang, Z., Guo, X., Liu, G., 2013. A review of the geological characteristics and mineralization history of iron deposits in the Altay orogenic belt of the Xinjiang, Northwest China. Ore Geol. Rev. 54, 1–16.
Yu, Y., Sun, M., Long, X., Li, P., Zhao, G., Kröner, A., Broussolle, A., Yang, J., 2017. Whole-rock Nd-Hf isotopic study of I-type and peraluminous granitic rocks from the Chinese Altai: Constraints on the nature of the lower crust and tectonic setting. Gondwana Res. 47, 131–141.
Yuan, C., Sun, M., Xiao, W.J., Li, X.H., Chen, H.L., Lin, S.F., Xia, X.P., Long, X.P., 2007. Accretionary orogenesis of the Chinese Altai: Insights from Paleozoic granitoids. Chem. Geol. 242, 22–39.
Yuan, H.L., Gao, S., Liu, X.M., Li, H.M., Gunther, D., Wu, F.Y., 2004. Accurate U-Pb age and trace element determinations of zircon by laser ablation-inductively coupled plasma mass spectrometry. Geostandards Newsl. 28, 353–370.
Yuan, F., Zhou, T.F., Yue, S.C., 2001. The ages and genetic types of the granites in the Nurt area, Altai. Xinjiang Geol. 19, 292–296 (in Chinese with English abstract).
Zagorsky, V.Y., 2007. Deep fluid flow-melt interaction and problems of granite-pegmatite system petrogenesis. Memórias Universidade do Porto 8, 58–59.
Zagorsky, V.Y., 2009. On emplacement of compositionally heterogeneous pegmatite melts: petrogenetic implications. Estudos Geológicos 19, 365–369.
Zagorsky, V.Y., Vladimirov, A.G., Makagon, V.M., Kuznetsova, L.G., Smirnov, S.Z., D'yachkov, B.A., Annikova, I.Y., Shokalsky, S.P., Uvarov, A.N., 2014. Large fields of spodumene pegmatites in the settings of rifting and postcollisional shear–pull-apart dislocations of continental lithosphere. Russian Geology and Geophysics 55, pp. 237–251.
Zhang, C., Liu, L.F., Santosh, M., Luo, Q., Zhang, X., 2017a. Sediment recycling and crustal growth in the Central Asian Orogenic Belt: Evidence from Sr–Nd–Hf isotopes and trace elements in granitoids of the Chinese Altay. Gondwana Res. 47, 142–160.
Zhang, J., Wang, T., Tong, Y., Zhang, Z., Song, P., Zhang, L., Huang, H., Guo, L., Hou, Z., 2017b. Tracking deep ancient crustal components by xenocrystic/inherited zircons of Palaeozoic felsic igneous rocks from the Altai-East Junggar terrane and adjacent regions, western Central Asian Orogenic Belt and its tectonic significance. Int. Geol. Rev. 1–20.
Zhang, X., Zhang, H., Ma, Z.L., Tang, Y., Lv, Z.H., Zhao, J.Y., Liu, Y.L., 2016. A new model for the granite–pegmatite genetic relationships in the Kaluan–Azubai–Qiongkuer pegmatite-related ore fields, the Chinese Altay. J. Asian Earth Sci. 124, 139–155.
Zhao, Z.H., Wang, Z.G., Zou, T.R., Masuda, A., 1993. The REE, isotopic composition of O, Pb, Sr and Nd and petrogenesis of granitoids in the Altai region. In: Tu, G.Z. (Ed.), Progress of Solid-Earth Sciences in Northern Xinjiang, China. Science Press, Beijing, pp. 239–266 (in Chinese with English abstract).
Zheng, C.Q., Kato, T., Enami, M., Xu, X.C., 2007. CHIME monazite ages of metasediments from the Altai orogen in northwestern China: Devonian and Permian ages of metamorphism and their significance. Island Arc 16, 598–604.
Zheng, J., Chai, F., Yang, F., 2016. The 401–409 Ma Xiaodonggou granitic intrusion: implications for understanding the Devonian Tectonics of the Northwest China Altai orogen. Int. Geol. Rev. 58, 540–555.
Zheng, Y., Chen, Y.J., Cawood, P.A., Wang, Y.J., Chen, H.Y., Zhang, L., Li, D.F., 2017. Late Permian-Triassic metallogeny in the Chinese Altay Orogen: Constraints from mica 40 Ar/39 Ar dating on ore deposits. Gondwana Res. 43, 4–16.
Zheng, Y., Zhang, L., Chen, Y.J., Qin, Y.J., Liu, C.F., 2012. Geology, fluid inclusion

geochemistry, and 40 Ar/39 Ar geochronology of the Wulasigou Cu deposit, and their implications for ore genesis, Altay, Xinjiang, China. Ore Geol. Rev. 49, 128–140.
Zheng, Y., Zhang, L., Li, D.F., Kapsiotis, A., Chen, Y.J., 2015. Genesis of the Dadonggou Pb–Zn deposit in Kelan basin, Altay, NW China: constraints from zircon U-Pb and biotite 40 Ar/39 Ar geochronological data. Ore Geology Rev. 64, 128–139.
Zhou, G., Zhang, Z.C., Luo, S.B., He, B., Wang, X., Yin, L.J., Zhao, H., Li, A.H., He, Y.K., 2007. Confirmation of high-temperature strongly peralumious Mayin'ebo granites in the south margin of Altay, Xinjiang: age, geochemistry and tectonic implications. Acta Petrologica Sinica 23, 1909–1920 (in Chinese with English abstract).
Zhou, Q.F., Qin, K.Z., Tang, D.M., Tian, Y., Cao, M.J., Wang, C.L., 2015. Formation age and evolution time span of the Koktokay No. 3 pegmatite, Altai, NW China: evidence from U-Pb zircon and 40Ar/39Ar muscovite ages. Resour. Geol. 65, 210–231.
Zhou, Q.F., Qin, K.Z., Tang, D.M., Wang, C.L. 2016. LA-ICP-MS U–Pb zircon, columbite-tantalite and 40Ar–39Ar muscovite age constraints for the rare-element pegmatite dykes in the Altai orogenic belt, NW China. Geological Magazine, 1-22.
Zhu, Y.F., Zeng, Y.S., Gu, L.B., 2006. Geochemistry of the rare metal-bearing pegmatite No. 3 vein and related granites in the Keketuohai region, Altay Mountains, northwest China. J. Asian Earth Sci. 27, 61–77.
Zhuang, Y.X., 1994. The pressure-temperature-space-time (PTSt) evolution of metamorphism and development mechanism of the thermal-structural-gneiss domes in the Chinese Altaides. Acta Geologica Sinica 68 (1), 35–47 (in Chinese with English abstract).
Zou, T.R., Li, Q.C., 2006. Rare and Rare Earth Metallic Deposits in Xinjiang, China. Beijing: Geological Publishing House 1–284 (in Chinese with English abstract).
Zou, T.R., Xu, J.G., 1975. On the origin and classification of granite pegmatites. Geochimica 3, 161–174 (in Chinese with English abstract).